Multimodel assessment of the factors driving stratospheric ozone evolution over the 21st century

L. D. Oman, D. A. Plummer, D. W. Waugh, J. Austin, J. F. Scinocca, A. R. Douglass, R. J. Salawitch, T. Canty, H. Akiyoshi, Slimane Bekki, et al.

Multimodel assessment of the factors driving stratospheric ozone evolution over the 21st century

L. D. Oman,[1,2] D. A. Plummer,[3] D. W. Waugh,[2] J. Austin,[4] J. F. Scinocca,[3] A. R. Douglass,[1] R. J. Salawitch,[5] T. Canty,[5] H. Akiyoshi,[6] S. Bekki,[7] P. Braesicke,[8] N. Butchart,[9] M. P. Chipperfield,[10] D. Cugnet,[7] S. Dhomse,[10] V. Eyring,[11] S. Frith,[1,12] S. C. Hardiman,[9] D. E. Kinnison,[13] J.-F. Lamarque,[13] E. Mancini,[14] M. Marchand,[7] M. Michou,[15] O. Morgenstern,[16] T. Nakamura,[6] J. E. Nielsen,[1,12] D. Olivié,[15] G. Pitari,[14] J. Pyle,[8] E. Rozanov,[17,18] T. G. Shepherd,[19] K. Shibata,[20] R. S. Stolarski,[1,2] H. Teyssèdre,[15] W. Tian,[10] Y. Yamashita,[6] and J. R. Ziemke[1,21]

Received 13 April 2010; revised 13 September 2010; accepted 23 September 2010; published 21 December 2010.

[1] The evolution of stratospheric ozone from 1960 to 2100 is examined in simulations from 14 chemistry-climate models, driven by prescribed levels of halogens and greenhouse gases. There is general agreement among the models that total column ozone reached a minimum around year 2000 at all latitudes, projected to be followed by an increase over the first half of the 21st century. In the second half of the 21st century, ozone is projected to continue increasing, level off, or even decrease depending on the latitude. Separation into partial columns above and below 20 hPa reveals that these latitudinal differences are almost completely caused by differences in the model projections of ozone in the lower stratosphere. At all latitudes, upper stratospheric ozone increases throughout the 21st century and is projected to return to 1960 levels well before the end of the century, although there is a spread among models in the dates that ozone returns to specific historical values. We find decreasing halogens and declining upper atmospheric temperatures, driven by increasing greenhouse gases, contribute almost equally to increases in upper stratospheric ozone. In the tropical lower stratosphere, an increase in upwelling causes a steady decrease in ozone through the 21st century, and total column ozone does not return to 1960 levels in most of the models. In contrast, lower stratospheric and total column ozone in middle and high latitudes increases during the 21st century, returning to 1960 levels well before the end of the century in most models.

Citation: Oman, L. D., et al. (2010), Multimodel assessment of the factors driving stratospheric ozone evolution over the 21st century, *J. Geophys. Res.*, *115*, D24306, doi:10.1029/2010JD014362.

1. Introduction

[2] Projecting the evolution of ozone in the 21st century is a critical issue. While changes in ozone are presently controlled primarily by declines in halogen concentrations, variations in temperature, circulation, and oxides of nitrogen and hydrogen also affect ozone [*World Meteorological Organization* (*WMO*), 2003, 2007]. Throughout the stratosphere, there will be long-term changes in various processes as well as the relative importance of these processes on

[1]NASA Goddard Space Flight Center, Greenbelt, Maryland, USA.
[2]Department of Earth and Planetary Sciences, Johns Hopkins University, Baltimore, Maryland, USA.
[3]Canadian Centre for Climate Modelling and Analysis, Victoria, British Columbia, Canada.
[4]NOAA Geophysical Fluid Dynamics Laboratory, Princeton, New Jersey, USA.
[5]Department of Chemistry and Biochemistry, University of Maryland, College Park, Maryland, USA.
[6]National Institute for Environmental Studies, Tsukuba, Japan.
[7]LATMOS-IPSL, UPMC, Paris, France.
[8]NCAS-Climate-Chemistry, Centre for Atmospheric Science, Department of Chemistry, University of Cambridge, Cambridge, UK.
[9]Met Office Hadley Centre, Exeter, UK.
[10]School of Earth and Environment, University of Leeds, Leeds, UK.
[11]Deutsches Zentrum für Luft- und Raumfahrt, Institut für Physik der Atmosphäre, Oberpfaffenhofen, Germany.
[12]Science Systems and Applications, Inc., Lanham, Maryland, USA.
[13]NCAR, Boulder, Colorado, USA.
[14]Dipartimento di Fisica, University of L'Aquila, L'Aquila, Italy.
[15]GAME/CNRM, Météo-France, CNRS, Toulouse, France.
[16]National Institute of Water and Atmospheric Research, Lauder, New Zealand.
[17]Physical-Meteorological Observatory Davos, World Radiation Center, Davos, Switzerland.
[18]IAC, ETHZ, Zurich, Switzerland.
[19]Department of Physics, University of Toronto, Toronto, Ontario, Canada.
[20]Meteorological Research Institute, Japan Meteorological Agency, Tsukuba, Japan.
[21]Goddard Earth Sciences and Technology Center, University of Maryland, Baltimore County, Catonsville, Maryland, USA.

0148-0227/10/2010JD014362

ozone. It is difficult to find a single approach to identify the contributions of different mechanisms affecting ozone levels throughout the stratosphere.

[3] Ozone loss throughout much of the stratosphere has been dominated by halogens, whose concentrations peaked around 1997 [e.g., *Yang et al.*, 2006; *Shepherd and Jonsson*, 2008; *Yang et al.*, 2008]. In the 21st century, as halogen concentrations are expected to decrease at about one-third of the rate of their increase in the late 20th century, other factors will likely play a more significant role in the evolution of ozone. Stratospheric cooling will decrease the rate of gas-phase reactions that destroy ozone and thereby increase concentrations of ozone [e.g., *Haigh and Pyle*, 1979; *Brasseur and Hitchman*, 1988; *Shindell et al.*, 1998; *Rosenfield et al.*, 2002]. The future increase in N_2O and CH_4 may cause loss of ozone by allowing nitrogen and hydrogen catalytic cycles to rise [e.g., *Randeniya et al.*, 2002; *Rosenfield et al.*, 2002; *Chipperfield and Feng*, 2003; *Portmann and Solomon*, 2007; *Ravishankara et al.*, 2009], but in a changing climate, stratospheric NO_y (or NO_x) may not increase proportionately to future rise in N_2O. *Rosenfield and Douglass* [1998] showed that NO_y loss rates increase as the stratosphere cools, decreasing the amount of NO_y produced per N_2O molecule and impacting future levels of ozone. Also, increased CH_4 concentrations act to increase globally integrated ozone amounts attributed to the direct production of ozone from methane oxidation in the troposphere and lower stratosphere [*Randeniya et al.*, 2002]. Several studies have linked increases in greenhouse gases (GHGs) to changes in stratospheric transport, further impacting ozone [*Waugh et al.*, 2009; *Li et al.*, 2009; *Hegglin and Shepherd*, 2009].

[4] *Eyring et al.* [2005] laid the groundwork for the Chemistry-Climate Model Validation (CCMVal) activity in which numerous chemistry-climate models (CCMs) were evaluated to increase our confidence in projecting future stratospheric ozone change. The results of the CCMVal-1 simulations of past ozone changes conducted for this activity were presented by *Eyring et al.* [2006], who evaluated processes important in determining the distribution of ozone. In a follow-up study, *Eyring et al.* [2007] presented the projections of stratospheric ozone change over the 21st century simulated by these CCMs and discussed how quantities that can impact ozone are projected to change.

[5] CCMVal-1 was the first major coordinated activity in which an ensemble of CCMs performed simulations with similar external forcings to assess ozone evolution [*Eyring et al.*, 2007]. The CCMVal-2 activity [*Eyring et al.*, 2008] included more models (14 are used here), and, in addition, more simulations cover the entire period of interest (1960–2100) than in CCMVal-1 (three models). Here we make use of CCMs that participated in the CCMVal-2 activity and that contributed projections of stratospheric ozone evolution until the end of the 21st century. These simulations are based on observed GHG and halogen concentrations in the past and on one projected scenario for the future.

[6] *Austin et al.* [2010a] examined the evolution of total column ozone and compared the dates ozone and Cl_y return to a particular historical level in the CCMVal-2 models. Here we (1) contrast the evolution of ozone in the upper and lower stratosphere and (2) examine the causes of the ozone changes (and differences among the models). Section 2 gives an overview of the models and model simulations. The results are discussed for extrapolar ozone in section 3 and polar ozone in section 4. Variations in ozone recovery by region are discussed in section 5, and a summary of the conclusions is given in section 6.

2. Models and Method

2.1. Model Simulations

[7] CCMVal-2 model simulations were conducted to improve the understanding of models through process-oriented evaluation along with discussion and coordinated analysis [*SPARC CCMVal*, 2010]. Information about individual model simulations and references for each are summarized in Table 1. In addition, *Morgenstern et al.* [2010] presented a much more detailed overview of the models that participated in this activity. Here we consider simulations from the CCMs that cover the years 1960 to 2099 (except Unified Model/United Kingdom Chemistry Aerosol Community Model–Met Office (UMUKCA-METO), which ends in 2083), with domains that include the upper stratosphere. Only these can be used to contrast the ozone evolution in the lower and upper stratosphere.

[8] Reference simulation REF-B2 uses the A1B GHG scenario from the *Intergovernmental Panel on Climate Change* (*IPCC*) [2000] and the revised A1 halogen scenario from *WMO* [2007; *SPARC CCMVal*, 2010]. The revised A1 halogen scenario includes the earlier phase out of hydrochlorofluorocarbons mandated by recent adjustments to the Montreal Protocol. For the Goddard Earth Observing System–Chemistry-Climate Model (GEOSCCM), a combination of REF-B1 (1960–2000) and REF-B2 (2001–2099) was used. REF-B1 differs only in that observed Hadley sea surface temperatures (SSTs) and sea ice data [*Rayner et al.*, 2003] were used instead of modeled SSTs. All model runs with the exception of the Canadian Middle Atmosphere Model (CMAM) use prescribed sea surface temperatures and sea ice extent. These SSTs and sea ice extent are based on fully coupled atmosphere-ocean runs for the A1B scenario, except for GEOSCCM, which uses observed SSTs and sea ice for 1960–2000 (see Table 1). CMAM includes a fully coupled ocean model in its simulations. All models use comprehensive stratospheric chemistry schemes except Atmospheric Model with Transport and Chemistry 3 (AMTRAC3), in which halogen-containing source gases are not explicitly modeled but, rather, Cl_y and Br_y are parameterized [*Austin and Wilson*, 2010; *Morgenstern et al.*, 2010]. REF-B2 simulations use background nonvolcanic aerosol loading, and there are no imposed solar cycle variations. Although several modeling groups submitted an ensemble of simulations, only the first member from each group was used in this analysis because as shown from CCMVal-1 simulations, the intermodel differences from these simulations are generally much larger than the ensemble spreads [*Eyring et al.*, 2007]. The annually averaged zonal mean is computed from the monthly zonal mean model output and used in this study. The partial and total column ozone amounts are integrated over the standard CCMVal-2 pressure levels.

[9] To view all 14 models on a single plot, filtering is necessary to remove short-term (e.g., high-frequency) variations. In all cases (except where noted), a 1:2:1 filter is used iteratively 30 times as described by *Eyring et al.* [2007] to smooth the model output displayed in Figures 1, 2, 3, 7,

Table 1. Model Description and References[a]

Model	Atmospheric GCM[b]	Domain/Resolution or Truncation	SST/Sea Ice for Ref-B2	Model Reference
AMTRAC3	AM3	Variable, ~200 km, 48 L, 0.017 hPa	CM2.1	*Austin and Wilson*, 2010
CAM3.5	CAM	1.9° × 2.5°, 26 L, 3.5 hPa	CCSM3	*Lamarque et al.*, 2008
CCSRNIES	CCSR/NIES AGCM 5.4g	T42, 34 L, 0.012 hPa	MIROC/IPCC-AR4	*Akiyoshi et al.*, 2009
CMAM	AGCM3	T31, 71 L, 0.00081 hPa	Interactive	*Scinocca et al.*, 2008; *de Grandpré et al.*, 2000
CNRM-ACM	ARPEGE- Climate version 4.6	T42, 60 L, 0.07 hPa	CNRM-CM3 AR4	*Déqué*, 2007); *Teyssèdre et al.*, 2007
GEOSCCM	GEOS5	2° × 2.5°, 72 L, 0.015 hPa	HadISST1 for Ref-B1 and CCSM3 for Ref-B2	*Pawson et al.*, 2008
LMDZrepro	LMDZ	2.5° × 3.75°, 50 L, 0.07 hPa	OPA (ocean), LIM (ice)	*Jourdain et al.*, 2008
MRI	MJ98	T42, 68 L, 0.01 hPa	MRI-CGCM2.3.2	*Shibata and Deushi*, 2008a, 2008b
SOCOL	MAECHAM4	T30, 39 L, 0.01 hPa	ECHAM5-MPIOM	*Schraner et al.*, 2008
ULAQ	ULAQ-GCM	R6/11.5° × 22.5°, 26 L, 0.04 hPa	CCSM3	*Pitari et al.*, 2002
UMSLIMCAT	HadAM3 L64	2.5° × 3.75°, 64 L, 0.01 hPa	HadGEM1	*Tian and Chipperfield*, 2005; *Tian et al.*, 2006
UMUKCA-METO	HadGEM-A	2.5° × 3.75°, 60 L, 84 km	HadGEM1	*Davies et al.*, 2005; *Morgenstern et al.*, 2009
UMUKCA-UCAM	HadGEM-A	2.5° × 3.75°, 60 L, 84 km	HadGEM1	*Davies et al.*, 2005; *Morgenstern et al.*, 2009
WACCM	CAM	1.9° × 2.5°, 66 L, 0.00000596 hPa	CCSM3	*Garcia et al.*, 2007

[a]HadGEM, Hadley Centre Global Environment Model; CAM, Community Atmosphere Model; MJ98, MRI/Japan Meteorological Agency 98; CCSM, Community Climate System Model; MIROC, Model for Interdisciplinary Research on Climate; MAECHAM4, Middle Atmosphere European Center/Hamburg version 4.
[b]GCM, general circulation model.

8, 9, and 10. This filter is only applied for graphics; all analyses use unfiltered data. The filter has a half-amplitude response of 21 years applied to annually averaged model output. While some differences can be seen in individual models between this filter and the time series additive-model analysis [*Scinocca et al.*, 2010], they are typically very small and do not impact our conclusions. The time series additive-model is a nonparametric additive model in which the trend estimate produces residuals that are independent, normally distributed random variables [*SPARC CCMVal*, 2010].

2.2. Multiple Linear Regression Analysis

[10] One of the primary methods we use to estimate the contribution of different mechanisms to the simulated changes in middle and upper stratospheric ozone is multiple linear regression (MLR). The method is explained in detail by *Oman et al.* [2010], but we repeat some of the basic details here. For a given location, MLR is applied to determine the coefficients m_X such that

$$\Delta O_3(t) = \sum_j m_{X_j} \Delta X_j(t) + \varepsilon(t), \quad (1)$$

where $\Delta O_3(t)$ are the annual mean ozone values, X_j are the different annual means of the quantities that could influence ozone, the coefficients m_X are the sensitivity of ozone to the quantities X(i.e., $m_X = \partial O_3/\partial X$), and ε is the residual in the fit. To do this, four explanatory variables (X_j) are used in (1): (1) $Cl_y+\alpha Br_y$, (2) reactive nitrogen (NO_y = NO + NO_2 + NO_3 + 2*(N_2O_5) + HNO_3 + HO_2NO_2 + $ClONO_2$ + $BrONO_2$), (3) reactive hydrogen (HO_x = OH+HO_2), and (4) temperature. Examples of the predictor time series can be seen in Figure 2 and have been smoothed for plotting purposes. Each term on the right side of equation (1) gives the "contribution" of the response in ozone caused by a change in X. We use $\alpha = 5$ in the definition as *Daniel et al.* [1999] showed this is an appropriate value for the upper stratosphere, which is the chemically driven region for which the MLR analysis is most appropriate. A test of this method using $\alpha = 60$ did not noticeably impact any of the individual contributions calculated in this study. We use $\alpha = 60$ in section 4, when examining polar lower stratospheric ozone changes, since a higher value of α is needed to represent the increased importance of bromine chemistry to polar ozone depletion. This value of 60 is based on the *WMO* [2007] recommendation for global ozone destruction and is similar to the value of 65 for polar ozone destruction given in *WMO* [2007].

[11] There are several limitations with the above linear regression approach, as discussed by *Oman et al.* [2010], that are summarized below. First, other mechanisms that are not considered in the regression (e.g., transport) could play a role. The role of transport on ozone is especially important in the lower stratosphere, and details of this complication are discussed in section 3.4. Second, significant correlations can exist between the temporal variations of the quantities, i.e., the quantities are not necessarily independent. Third, a high correlation between ozone and a quantity does not show causality, as ozone could be causing the quantity to change, or changes in another quantity could be causing both ozone and the quantity of interest to change in a correlated way. Temperature and ozone in the upper stratosphere are an example of this third complication, e.g., changes in ozone cause variations in temperature through changes in shortwave heating [*Shine et al.*, 2003]. At the same time, the local ozone concentration responds to variations in temperature, because the chemical reaction rates are temperature dependent. Also, the relationship between the regression variables

and ozone may not be linear. For example, the ClO/Cl_y ratio varies as a function of temperature in a highly nonlinear manner. One could use a regression based on the rates of odd-oxygen loss by nitrogen, chlorine, and bromine radical abundances as regressor variables, as was done by *Yang et al.* [2006]. However, this treatment is beyond the scope of the present analysis, as the information archived by each model makes the use of radical abundances challenging to implement. Because of the above limitations, caution must be applied when interpreting the MLR results presented below.

[12] UMUKCA-UCAM and AMTRAC3 did not provide HO_x, so for these models the MLR consists of three explanatory variables. This analysis has been repeated without HO_x for all models, and while there is some decrease in explained variance from the MLR, the main findings and conclusions are not impacted.

3. Extrapolar Ozone

3.1. Total Column Ozone

[13] *Austin et al.* [2010a] examined the changes in total column ozone in the CCMVal-2 simulations. Here we start with total column ozone and then break down the ozone amounts into two partial columns for the extrapolar region. Figures 1a–1c show the evolution of total column ozone amounts over the tropics (25°S–25°N) and midlatitudes of each hemisphere (35°–60°S and 35°–60°N), for each of the CCMVal-2 models. The evolution is shown with respect to 1960 levels and has been smoothed as described above. Also shown is the evolution of ground-based total column ozone measurements (black squares; updated from *Fioletov et al.* [2002]) with respect to the smoothed 1964 value, the first year of the data set. The difference between 1960 and 1964 ozone values is not expected to be significant. Total and partial column ozone measurements are from the Total and Profile Merged Ozone Data Set (MOD) [*Stolarski and Frith*, 2006; *Ziemke et al.*, 2005] (http://acdb-ext.gsfc.nasa.gov/Data_services/merged/index.html). The Total MOD includes observations from the Nimbus 7 and Earth Probe Total Ozone Mapping Spectrometer instruments, from the solar backscatter ultraviolet (SBUV and SBUV2) series of instruments, and the Aura Ozone Monitoring Instrument. The Profile MOD, hereafter referred to as SBUV MOD, includes profile data from the SBUV instruments. The upper partial column is constructed from integrated SBUV MOD data from 20 to 1 hPa. The lower partial column is computed by subtracting the upper partial column from the Total MOD observations. Total Ozone Mapping Spectrometer, SBUV, and Ozone Monitoring Instrument are all nadir-viewing instruments and only make measurements over sunlit portions of the globe. No measurements are available during polar night. One issue is that using 1979 as a reference year may not be the best comparison to models referenced to 1960. However, for the extrapolar regions plotted in Figure 1, we note that total column ozone amounts between this and the ground-based data set agree to within 2 Dobson units (DU) in 1979; this was also found by *Fioletov et al.* [2002]. We reference the models to 1960 because important differences have emerged by 1980, because significant increases in halogens have occurred by 1980.

[14] There is qualitative agreement in the evolution of ozone among regions and models at the broadest level, with ozone decreasing from 1960 to around 2000, and then increasing in the first half of the 21st century [*Austin et al.*, 2010a]. All models consistently indicate tropical total column ozone at the end of the 21st century is less than it was in 1960 (Figure 1b). In contrast, total column ozone over the midlatitudes (Figures 1a and 1c) in 2100 exceeds 1960 values in nearly all the models, with a generally larger increase in Northern Hemisphere (NH) midlatitudes.

[15] There is a large spread in the magnitude of the peak ozone loss (around 2000) and the date that column ozone is projected to return to 1960 levels. For example, in Southern Hemisphere (SH) midlatitudes, the simulated decrease in ozone from 1960 to 2000 varies from around 10 DU to over 50 DU, while the date of return to 1960 levels for the same region varies from around 2030 to after 2100. In all three latitude bands, Centre National Recherche Meteorologique–ARPEGE-Climat coupled MOCAGE (CNRM-ACM) and Meteorological Research Institute (MRI) show the largest loss in total column ozone by the year 2000 and also tend to have later return dates. UMUKCA-METO has the smallest ozone loss in the tropics and SH and one of the smallest decreases in NH midlatitudes. The reasons for these model differences are examined in section 3.2. Also, there is a large difference in the ozone decline in the SH midlatitudes prior to 1975 found by the various models (declines ranging from 0 to 20 DU), with no change over this time period apparent in the ground-based ozone observations. Ground-based total column ozone observations indicate about a 20 DU decrease by 2000 in the SH midlatitudes and about a 15 DU decrease in the NH midlatitudes with similar decreases in the SBUV MOD observations. In the tropics, the small observed column ozone changes are similar to those produced by UMUKCA-METO but are less than the ozone changes simulated by all other models.

3.2. Partial Column Ozone

[16] It is useful to look at changes in the partial columns [e.g., *Yang et al.*, 2006; *Li et al.*, 2009] to understand the relative role of changes in the upper and lower portions of the stratosphere in the differences described above. As described by *Oman et al.* [2010], we split the stratosphere at 20 hPa because the ozone changes at 20 hPa are generally small and 20 hPa separates the photochemically controlled ozone region above from the transport and chemically driven region below. Other studies have used 15 hPa [e.g., *Li et al.*, 2009] or 25 km altitude (~25 hPa) [e.g., *Yang et al.*, 2006], but we prefer 20 hPa, as used by *Oman et al.* [2010]. The results presented are not sensitive to the precise specification of the pressure chosen to distinguish the upper and lower partial columns within the range of these previous studies. CAM3.5 has a model top at 3.5 hPa, which could impact the model's upper stratospheric ozone projection.

[17] Figures 1d–1f and 1g–1i show the evolution of the partial column ozone amounts for the upper (20–0.1 hPa) and lower (500–20 hPa) portions of the column. The evolution in the upper partial column ozone is similar among the three regions, but there are significant differences in the lower partial column. It is the differences in the lower stratosphere that cause differences in the evolution of column ozone among regions. In particular, the decrease in

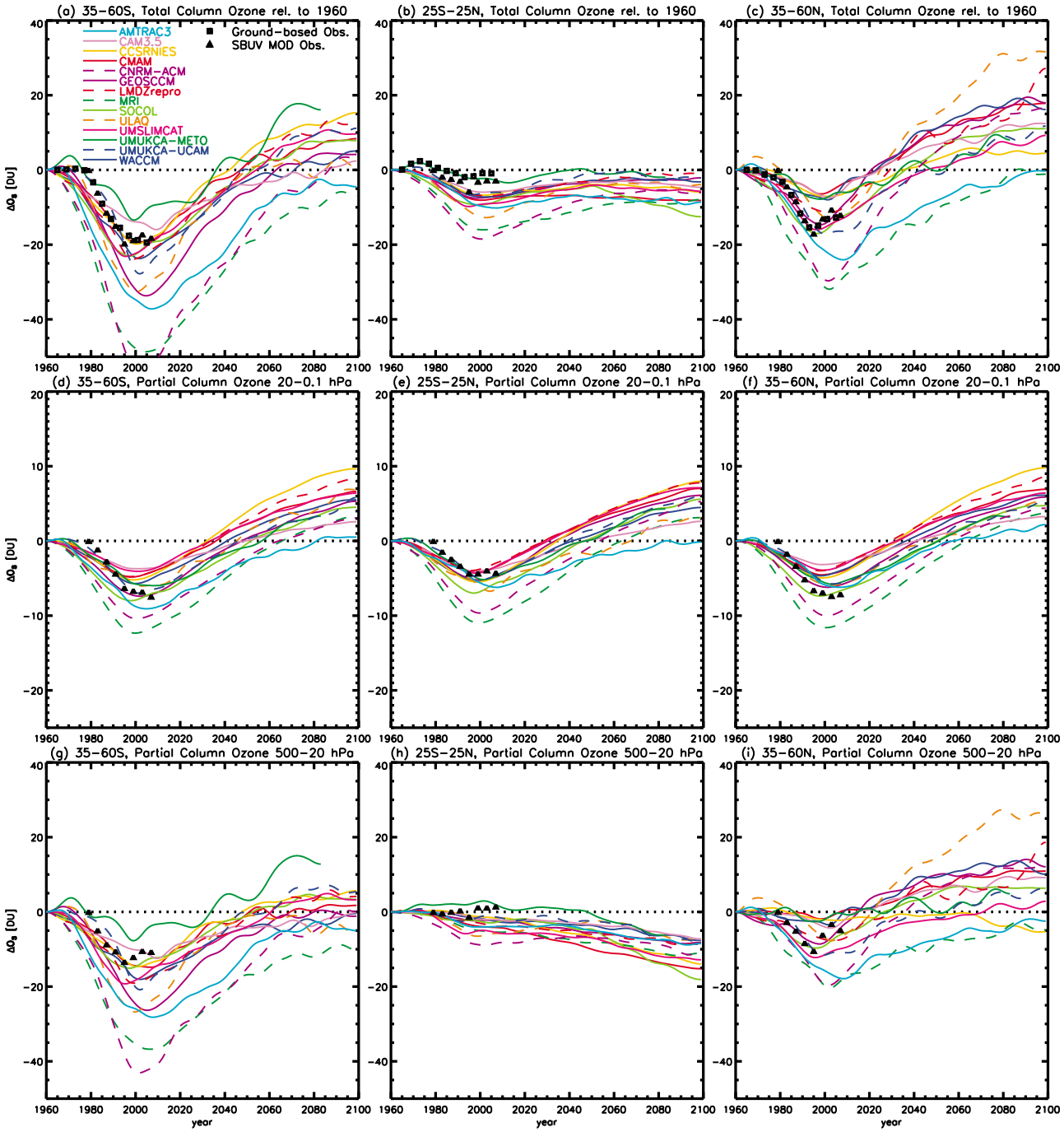

Figure 1. Annual average (a–c) total and (d–i) partial column ozone amounts over three regions including the tropics (25°S–25°N) and midlatitudes of each hemisphere (35°–60°S and 35°–60°N). The partial column ozone is separated into an upper portion (Figures 1d–1f) from 20 to 0.1 hPa and a lower portion (Figures 1g–1i) from 500 to 20 hPa. All output are from 1960 to 2100 (except UMUKCA-METO to 2083) and have been smoothed with a 1:2:1 filter iteratively 30 times. Note the scale change in the *y* axis in Figures 1d–1f, which are half the magnitude of the other panels. Ground-based total column ozone observations (black squares; plotted every 4th year) are shown over 1964–2007 relative to 1964. SBUV MOD total and partial column ozone observations (black triangles; plotted every 4th year) are shown over 1979–2009 relative to 1979.

tropical column ozone over the latter half of the 21st century is due to decreases in the lower stratosphere (Figure 1h), which are larger than increases in upper stratospheric ozone (Figure 1e).

[18] Models with larger (smaller) total column ozone changes around year 2000 generally have larger (smaller) changes in both lower and upper partial columns. There are quantitative differences in the upper columns, but these are

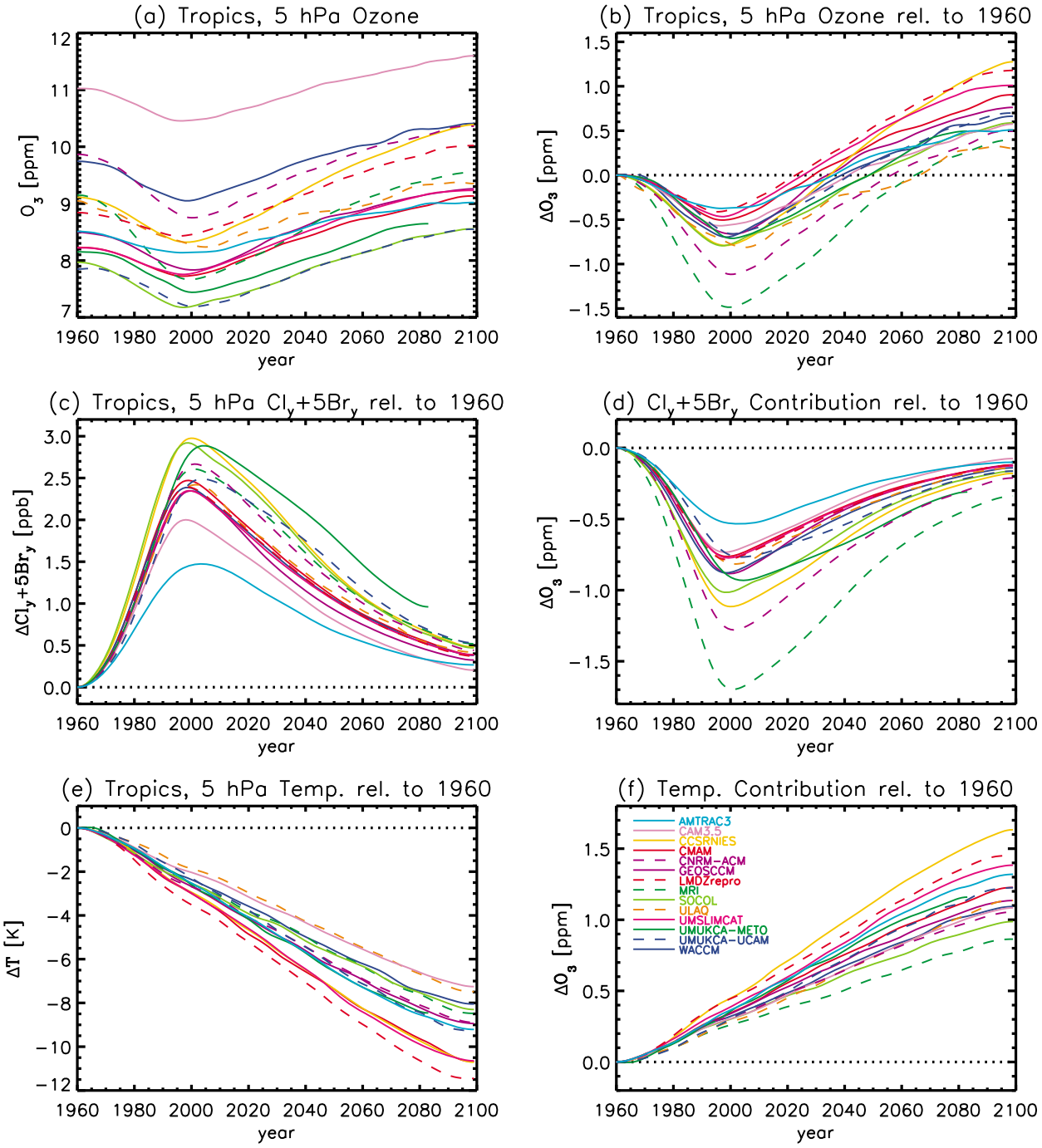

Figure 2. (a) Evolution of ozone in the tropics (25°S–25°N) at 5 hPa and (b) change in ozone with respect to 1960 levels for the CCMVal models. Models change in (c) Cl_y + $5Br_y$ and (e) temperature with respect to 1960 levels. Ozone changes congruent with changes in (d) Cl_y + $5Br_y$ and (f) temperature. All models are shown from 1960 to 2100 (except UMUKCA-METO to 2083) and have been smoothed with a 1:2:1 filter iteratively 30 times. Model evolution of (g) NO_y and (i) HO_x with respect to 1960 levels over (25°S–25°N) at 5 hPa. Ozone changes congruent with changes in (h) NO_y and (j) HO_x. All models are shown from 1960 to 2100 (except UMUKCA-METO to 2083) and have been smoothed with a 1:2:1 filter iteratively 30 times.

generally smaller than the differences in the lower columns, especially in midlatitudes (note the different scales for upper and lower column plots in Figure 1). Peak losses occur around the year 2000, with a range of 3–7 DU over the tropics and midlatitudes for the upper partial column of most models, although MRI and CNRM-ACM have larger losses of around 10 DU. Observations over these three latitude bands indicate a decrease of 5–7 DU from 1979. In the

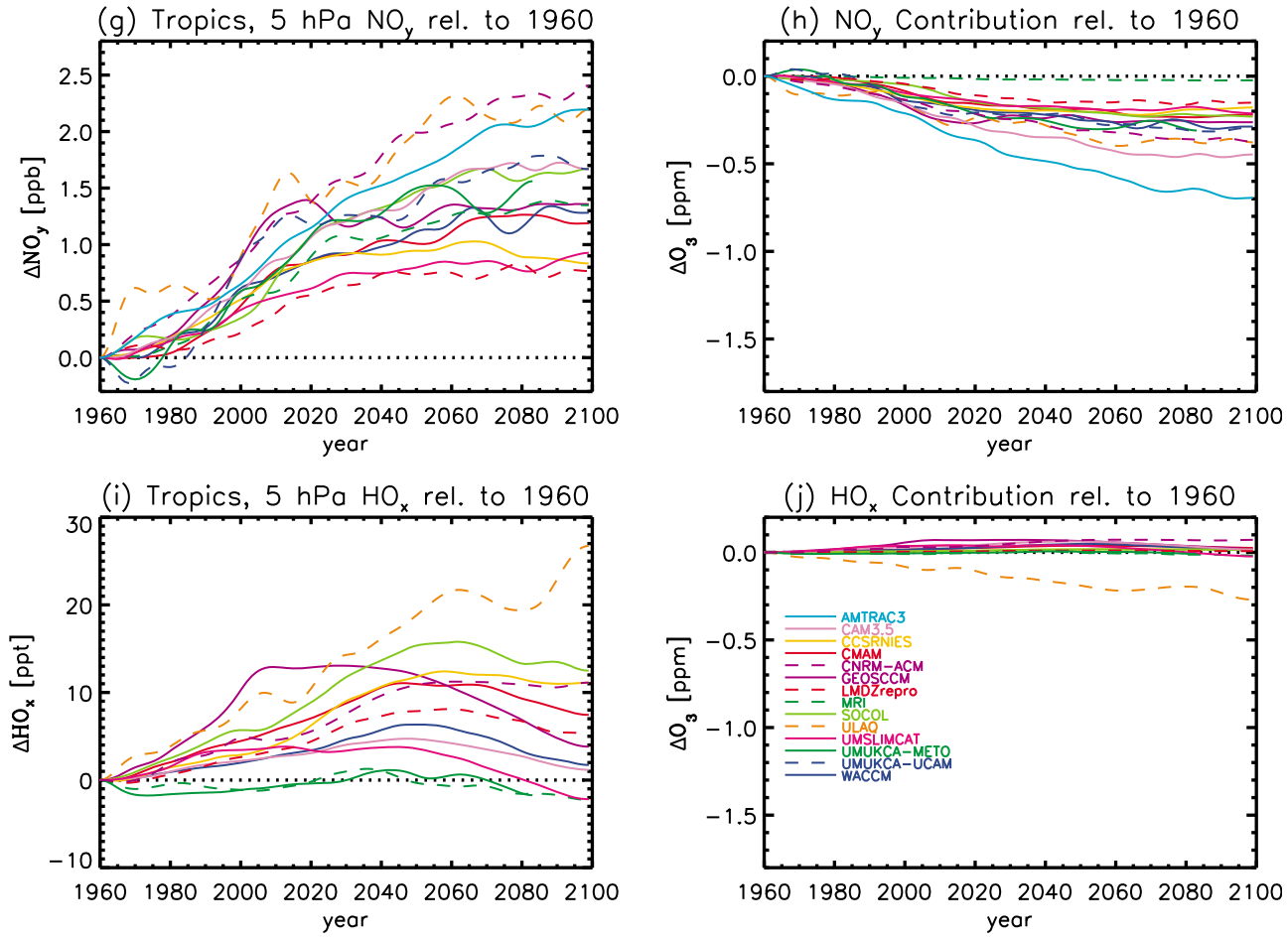

Figure 2. (continued)

lower partial column, there are much greater differences in the ozone change over this range of latitudes. Midlatitude ozone losses around 2000 are largest in the SH, as expected because of the effects of the Antarctic ozone hole [*Atkinson et al.*, 1989]. Ozone losses range from 10 to 25 DU over most models with less ozone loss in UMUKCA-METO and significantly more in MRI and CNRM-ACM. Tropical latitudes show the largest loss of ozone by the end of the 21st century, with a range of 7–18 DU, with most models showing between 2 to 5 DU loss by 2010 from the 1960 reference. SBUV MOD observations do not show a trend in the partial lower stratosphere column ozone over the 1979–2009 time period. *Randel and Wu* [2007] reported negative trends in tropical lower stratospheric ozone using Stratospheric Aerosol and Gas Experiment (SAGE) I and SAGE II data over a similar time period, suggesting further study is needed to reconcile these differences [*WMO*, 2007]. The tropical lower partial column is the only region where ozone is projected to continue to decline until the end of the 21st century, because of increased strength of the Brewer-Dobson circulation in the models that is driven by rising GHG concentrations [*Rind et al.*, 1998; *Butchart and Scaife*, 2001; *Butchart et al.*, 2006; *Shepherd*, 2008; *Li et al.*, 2009; *Garcia and Randel* [2008]; *Akiyoshi et al.*, 2010]. An increase in the circulation of the stratosphere reduces the transit time of an air parcel through the tropical lower stratosphere, resulting in lower values of ozone because of less time for accumulation of the ozone that is produced in this region [*Avallone and Prather*, 1996].

3.3. Upper Stratosphere

[19] As discussed above, and shown in Figures 1d–1f, the evolution of ozone in the upper portion of the stratosphere is qualitatively similar among most models. Also, the overall behavior of ozone in the tropics and midlatitudes (both hemispheres) is similar. Nonetheless, there are quantitative differences among the models. We use the MLR analysis described in section 2 to examine which explanatory variables are causing the ozone changes and the differences among the models.

[20] We consider first the evolution of ozone at 5 hPa in the tropics (25°S–25°N). Figure 2a shows the evolution of the ozone mixing ratio, while Figure 2b shows the change in ozone with respect to 1960 levels. There is a large spread in the time-mean values of ozone among the models (from around 8 ppmv to around 11 ppmv) and also some differences in changes relative to 1960 levels. All models show a peak ozone loss around 2000, with magnitudes of 0.5 and 0.7 ppm for most models. This peak ozone loss coincides with the peak chlorine loading, which is specified by the

boundary conditions. The MRI and CNRM-ACM models show the largest peak ozone loss (greater than 1.0 ppm), whereas AMTRAC3 and Laboratoire de Météorologie Dynamique Zoom–REPROBUS (LMDZrepro) have the smallest loss (less than 0.4 ppm). All models also show 5 hPa ozone returning to 1960 levels before the end of the 21st century, but there is a large spread in dates when this occurs (from early 2020s to 2060s).

[21] As presented in the Introduction, several mechanisms can cause changes in ozone, including changes in halogens, temperature, reactive nitrogen and hydrogen, and transport. Figures 2c, 2e, 2g, and 2i show the evolution of $Cl_y + \alpha Br_y$, temperature, NO_y, and HO_x, respectively. The evolution of $Cl_y + \alpha Br_y$ and variation among models (Figure 2c) is somewhat similar to that of ozone (Figure 2a), suggesting that differences in $Cl_y + \alpha Br_y$ can explain much of the ozone evolution. However, there is not a simple one-to-one relationship between changes in ozone and those in $Cl_y + \alpha Br_y$. For instance, ozone exceeds 1960s values in the later part of the 21st century, while $Cl_y + \alpha Br_y$ is still above 1960 levels. Also, models with larger values of $Cl_y + \alpha Br_y$ (Figure 2c) do not necessarily have larger ozone loss, e.g., MRI and CNRM-ACM have the largest peaks in ozone loss but do not have the largest changes in $Cl_y + \alpha Br_y$.

[22] One possible cause for the lack of a simple relationship between ozone and halogen changes is differences in temperature trends. As shown in Figure 2e, all models show cooling throughout the 21st century, largely from increasing CO_2 concentrations [*Shindell et al.*, 1998], and this is expected to increase ozone (by slowing down the gas phase rate of reactions that destroy ozone). However, it should be noted that over the recent past about 50% of the cooling is associated with the ozone loss from $Cl_y + \alpha Br_y$ [*Shepherd and Jonsson*, 2008]. The simulated future cooling, mostly from increasing CO_2 concentrations, explains the increase in ozone above 1960 levels before $Cl_y + \alpha Br_y$ returns to 1960 values. Most models cool by about 8–9 K below 1960 levels by the end of century, but a few models have cooling exceeding 10 K (Center for Climate System Research/National Institute for Environmental Studies (CCSRNIES), Unified Model–SLIMCAT (UMSLIMCAT), LMDZrepro, and CMAM). These four models have among the largest ozone increases by 2100, which is consistent with an expected increase in ozone attributed to cooling, as shown in Figure 2b.

[23] To quantify the relative contributions of the above mechanisms to ozone changes, we now apply an MLR analysis to model outputs. As described in section 2, the MLR analysis is used to quantify the contributions of changes in $Cl_y + \alpha Br_y$, temperature, NO_y, and HO_x to the ozone changes. An example of the correlation coefficient squared, R^2, between the modeled ozone time series and the MLR is shown in the study by *Oman et al.* [2010; their Figure 4]. Typically, the regression explains more than 90% of the variance ($R^2 > 0.9$) throughout much of the upper stratosphere (above 10 hPa). Poleward of 60° latitude, and in the lower stratosphere (100–10 hPa), the regression typically explains less than 80% of the variance. In these regions, regression results are less reliable. As previously discussed in section 2, there are a number of caveats with this type of analysis, and care should be taken in interpreting the results. The MLR analysis is performed on the annual average model output, which takes advantage of both short-term (interannual) variability and long-term trends in separating the relative contributions. This MLR analysis has been compared and agrees well with chemical box model calculations in the upper stratosphere for the GEOSCCM [*Oman et al.*, 2010].

[24] The contributions from $Cl_y + \alpha Br_y$, temperature, NO_y, and HO_x are shown in Figures 2d, 2f, 2h, and 2j, respectively. Differences among models in the contribution from $Cl_y + \alpha Br_y$ are generally similar to relative variations in $Cl_y + \alpha Br_y$ (compare Figures 2d and 2c), with some exceptions. Most notably, MRI and CNRM-ACM have the largest ozone loss at this level from 1960 to 2000 despite not having unusually large amounts of $Cl_y + \alpha Br_y$. This is related to larger sensitivities to $Cl_y + \alpha Br_y$, and we quantify this sensitivity below.

[25] Temperature trends play an important role in the return of ozone to above historical levels: the four models with the largest cooling trend (LMDZrepro, CCSRNIES, CMAM, and UMSLIMCAT) (Figure 2e) have the largest increases in ozone relative to 1960 levels (see Figure 2b). The differences in cooling among models explain most of the variation in projected ozone by 2100, although, again, we note that there is not a simple one-to-one relationship between ozone and temperature.

[26] The contributions of NO_y and HO_x to changes in ozone are significantly smaller in most cases. Figures 2h and 2j show the contributions of NO_y and HO_x to ozone changes. For NO_y, most models show losses of 0.2–0.3 ppm by 2100 with a few models showing somewhat larger loss, up to a loss of 0.7 ppm in AMTRAC3. While 5 hPa is typically one of the largest loss regions from NO_y changes in volume mixing ratio, HO_x has a much smaller impact at this level and typically is more important at pressures lower than 5 hPa [*Jackman et al.*, 1986]. All models show a relatively small contribution (less than 0.1 ppm) from HO_x except Universitá degli Studi dell'Aquila (ULAQ), which has the largest HO_x trend (Figure 2i). ULAQ has one of the largest temperature trends at the tropical tropopause, so stratospheric water vapor increases more in their model than the others, which could be related to the coarser model resolution. In general, for the A1B GHG scenario considered in these CCMVal-2 simulations, NO_y and HO_x contributions are much smaller than the contributions from halogen recovery and stratospheric cooling over the 21st century. However, this may not be the case for other possible future scenarios for N_2O and CH_4 [e.g., *Oman et al.*, 2010].

[27] The above analysis indicates, for the GHG and halogen scenario considered, that changes in $Cl_y + \alpha Br_y$ and temperature dominate tropical ozone evolution at 5 hPa, and differences in the simulated changes in these quantities explain most (but not all) of the variations among the models. However, by 2100 at 5 hPa, temperature and NO_y generally show the largest contribution to the change in ozone with respect to 1960 values. Table 2 shows, for all 14 models, the numerical values of the individual sensitivity coefficients, m_X, and the 3σ uncertainty of the fit for 25°S–25°N at 5 hPa. This was shown in tropical profile form by *Oman et al.* [2010] and agrees well, in general, with the results presented here. HO_x is not a significant driver of ozone variability at 5 hPa, which is consistent with these results as the sensitivity for about half of the models is not

Table 2. Sensitivity Coefficients and Their 3σ Uncertainty of the Fit for 25°S–25°N, 5 hPa

Model	Cly + αBry (ppm/ppb)	Temperature (ppm/K)	NO_y (ppm/ppb)	HO_x (ppm/ppt)
AMTRAC3	−0.36 ± 0.09	−0.14 ± 0.04	−0.31 ± 0.16	N/A
CAM3.5	−0.37 ± 0.01	−0.15 ± 0.01	−0.27 ± 0.02	0.013 ± 0.004
CCSRNIES	−0.37 ± 0.01	−0.15 ± 0.01	−0.21 ± 0.03	0.001 ± 0.003
CMAM	−0.31 ± 0.01	−0.12 ± 0.01	−0.19 ± 0.02	0.003 ± 0.002
CNRM-ACM	−0.48 ± 0.02	−0.12 ± 0.02	−0.16 ± 0.07	0.006 ± 0.014
GEOSCCM	−0.38 ± 0.01	−0.13 ± 0.01	−0.19 ± 0.01	0.005 ± 0.001
LMDZrepro	−0.33 ± 0.01	−0.13 ± 0.01	−0.20 ± 0.02	0.001 ± 0.003
MRI	−0.65 ± 0.03	−0.10 ± 0.02	−0.02 ± 0.07	0.008 ± 0.019
SOCOL	−0.35 ± 0.01	−0.12 ± 0.01	−0.14 ± 0.04	0.001 ± 0.004
ULAQ	−0.34 ± 0.02	−0.15 ± 0.02	−0.17 ± 0.03	−0.010 ± 0.006
UMSLIMCAT	−0.33 ± 0.02	−0.13 ± 0.01	−0.23 ± 0.05	0.011 ± 0.007
UMUKCA-METO	−0.32 ± 0.01	−0.14 ± 0.01	−0.20 ± 0.03	0.005 ± 0.009
UMUKCA-UCAM	−0.31 ± 0.02	−0.13 ± 0.01	−0.18 ± 0.04	N/A
WACCM	−0.37 ± 0.01	−0.14 ± 0.01	−0.22 ± 0.03	0.008 ± 0.004

statistically significantly different from zero. NO_y coefficients, with the exception of that from MRI, are all significantly different from zero but do have more uncertainty than the remaining explanatory variables. To see how representative the changes at 5 hPa are over a range of pressures, Figure 3 shows vertical profiles of changes between 2000 and 2100 for 25°S–25°N.

[28] Figure 3a shows each model's reference ozone profile for the year 2000, while changes by 2100 appear in Figure 3b. Also plotted on Figure 3a are Microwave Limb Sounder (MLS) satellite measurements (black squares) averaged from 2005 to 2009. The peak ozone increase is typically at 3 hPa (Figure 3b) with most models centered at around 1.5 ppm. Figure 3c shows that in the upper stratosphere, most models have a $Cl_y + \alpha Br_y$ decrease of 2 ppb over this time period. CCSRNIES and Solar-Climate-Ozone Links (SOCOL) have larger than average decreases in $Cl_y + \alpha Br_y$, and AMTRAC3 has a smaller than average $Cl_y + \alpha Br_y$ change with a different vertical structure that is not consistent with observations, which is due to how AMTRAC3 treats the breakdown of halogens. Again, we see that MRI and CNRM-ACM have the largest ozone changes caused by $Cl_y + \alpha Br_y$ (Figure 3d), with AMTRAC3 having the smallest increase over the upper stratosphere. Most models show about equal contributions from decreases in $Cl_y + \alpha Br_y$ and decreases in temperature to the ozone increases over the 21st century. Observations from the MLS [*Santee et al.*, 2008a] for HCl (data not shown) suggest that while a few models are in good agreement with MLS in the upper stratosphere, many appear to be on the low end with only CCSRNIES on the high end of observations. Possible causes for these differences include differences in the number of Cl species included in the models, as well as conservation issues in a few models [*SPARC CCMVal*, 2010].

[29] Figure 3 shows that the key features seen at 5 hPa hold throughout the upper stratosphere (10–1 hPa). Models that have high (low) ozone changes at 5 hPa have similar characteristics throughout the upper stratosphere. Also, differences in $Cl_y + \alpha Br_y$ can explain most of the variations among the models with additional contributions from temperature. Figure 3h shows the contribution from NO_y to changes in ozone: it is typically much smaller, and opposite in sign, than changes caused by $Cl_y + \alpha Br_y$ or temperature. In general, models show NO_y-related ozone loss of 0.2 ppm around 3–10 hPa, with only AMTRAC3 exhibiting a larger loss. As presented in the Introduction, stratospheric cooling increases loss of NO_y [*Rosenfield and Douglass*, 1998], causing a smaller increase (and even some decreases) (Figure 3g) in NO_y over the 21st century than would be expected from N_2O increases in the absence of climate change. The interpretation of changes in lower stratospheric ozone is complicated by the increasingly important impact of transport, which is not explicitly included in the MLR analysis and will be discussed in more detail in section 3.4.

[30] As discussed above, there are not always one-to-one relationships between changes in $Cl_y + \alpha Br_y$ and temperature and their contribution to ozone changes. One possible reason for this is the different sensitivities of ozone to $Cl_y + \alpha Br_y$ and temperature. That is, a unit of change in the explanatory variable can lead to a slightly different ozone change in each model. Figure 4 shows the vertical profiles of the sensitivity of tropical ozone (25°S–25°N) to $Cl_y + \alpha Br_y$, temperature, and NO_y calculated over the period 1960–2100. Overall, there is good agreement between the sensitivities of the various models. All models show a peak $Cl_y + \alpha Br_y$ sensitivity at 3 hPa, mostly around −0.35 ppm/ppb. However, two models stand out with much larger sensitivities, CNRM-ACM (−0.6 ppm/ppb) and MRI (−0.8 ppm/ppb) at 3 hPa. Also plotted on Figure 4 (black Xs) are the chemical box model calculations for July at 2°N shown and described by *Oman et al.* [2010]. The differences are very similar to those seen by *Oman et al.* [2010], with the best agreement seen from 0.9 to 2.9 hPa and with slightly higher sensitivities seen at 5.6 and 6.9 hPa in the box model calculations compared to most models.

[31] Further insight into the sensitivity of modeled ozone to $Cl_y + \alpha Br_y$ can be gained by examining the abundance of ClO and BrO archived by the various CCMs. Here we provide a snapshot of the analysis presented in chapter 6 of *SPARC CCMVal* [2010]. Figure 5 shows profiles of the ClO/Cl_y ratio archived by four of the CCMs at 35°N for September 1993 and at 22°N for February 1996 (colored lines). The black lines represent the calculated ratio of ClO/Cl_y found using a photochemical steady state (PSS) box model [e.g., *Canty et al.*, 2006, and references therein) constrained by fields of O_3, H_2O, CH_4, Cl_y, NO_y, aerosol surface area, and other constituents archived by each CCM group. Results are shown for four models: the two in question (MRI and CNRM-ACM) and two that archive ClO values that are well explained by the PSS simulation (CMAM and Whole-Atmosphere Chemistry-Climate Model (WACCM)). The numerical value on each panel is

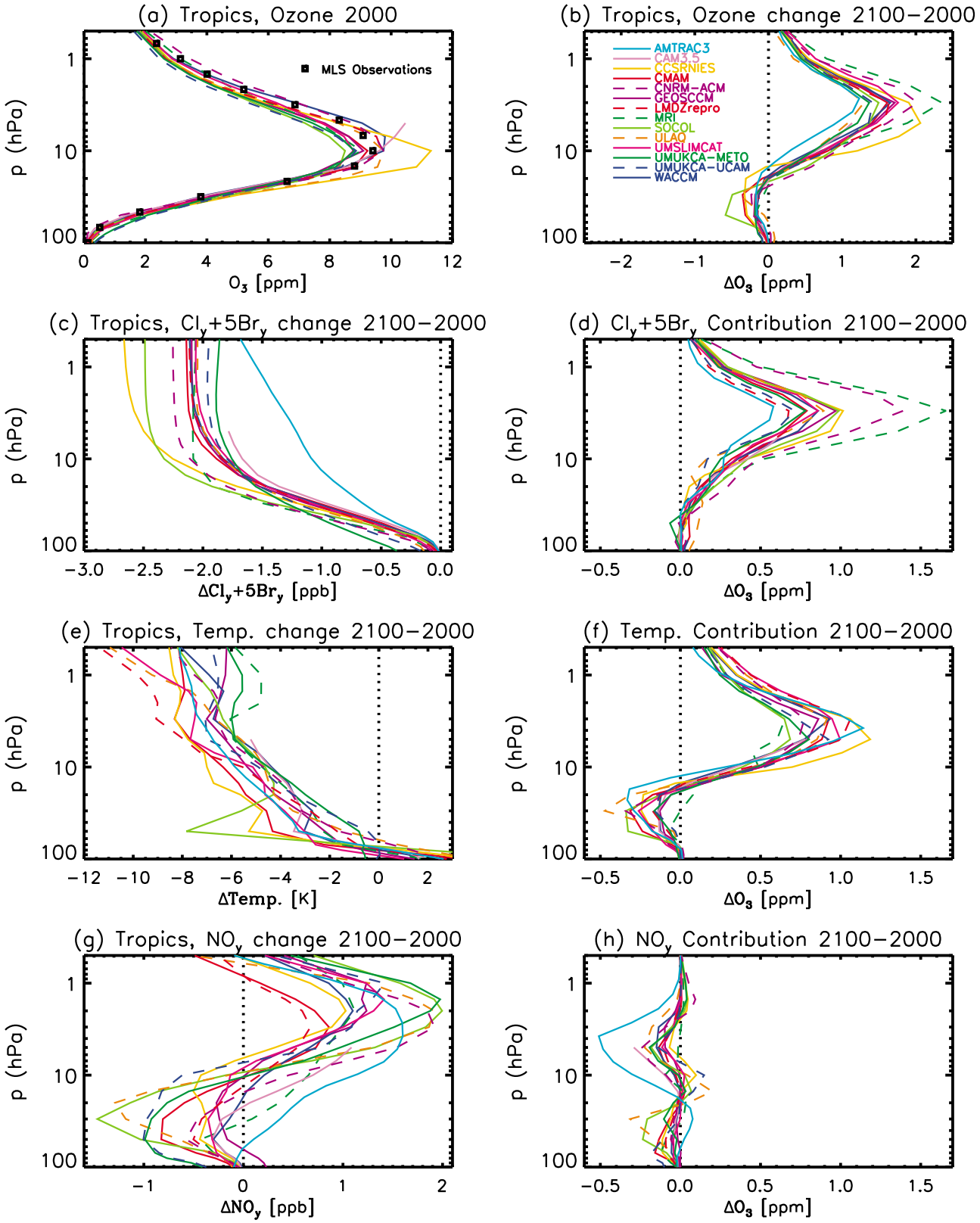

Figure 3. (a) Profiles of ozone in the tropics (25°S–25°N) for 2000 and (b) differences in ozone from 2000 to 2100 for the CCMVal models. Model differences in (c) $Cl_y + 5Br_y$, (e) temperature, and (g) NO_y from 2000 to 2100. Also shown are the ozone changes congruent with changes in (d) $Cl_y + 5Br_y$, (f) temperature, and (h) NO_y, except UMUKCA-METO change shown from 2000 to 2083. Also shown in Figure 3a are observations from MLS (black squares) for reference.

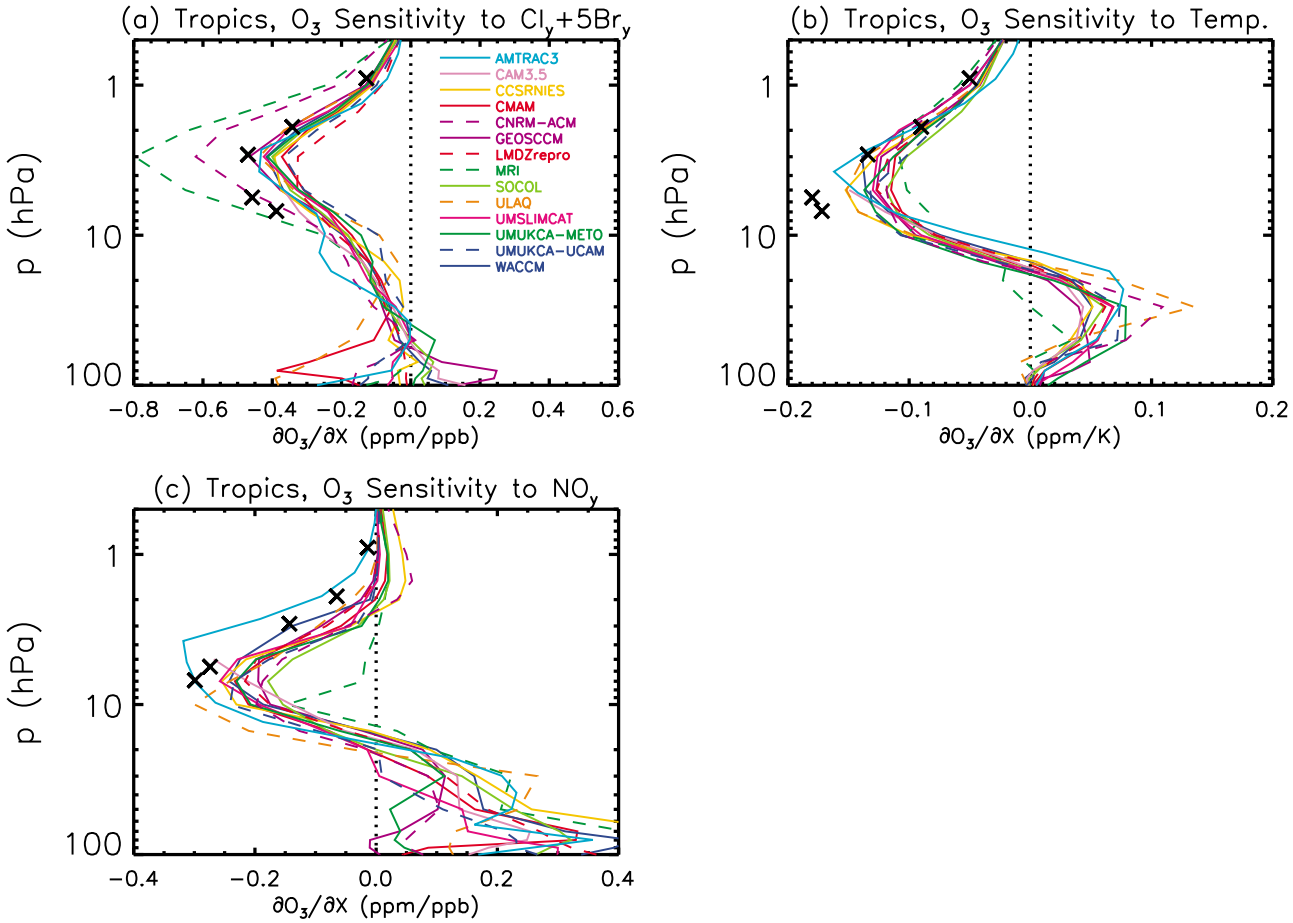

Figure 4. Tropical (25°S–25°N) profiles of the sensitivity of ozone to changes in (a) $Cl_y + 5Br_y$ (ppm/ppb), (b) temperature (ppm/K), and (c) NO_y (ppm/ppb). The black Xs are the chemical box model calculations described by *Oman et al.* [2010].

the "metric" assigned to each comparison, with a value of unity indicating perfect agreement with the PSS simulation.

[32] The profiles of ClO archived by CMAM and WACCM are in excellent agreement with the PSS simulation, indicating that implementation of the chemical mechanism within these models agrees well with the implementation of the mechanism within the PSS model. However, the MRI ClO profile is much higher (Figure 5, green dashed line) than the profile found using the PSS model. As explained in the *SPARC CCMVal* [2010] study, the MRI chemical mechanism neglected the channel for the loss of ClO by the reaction of ClO + OH to yield HCl + O_2. This leads to much higher values of ClO than are reported by other models or observed in the atmosphere [*Santee et al.*, 2008b]. Even when we neglect this reaction channel in our PSS model (Figure 5, black dotted curves), we still cannot account for the high values of ClO archived by the MRI group. We conclude that the high sensitivity of O_3 to $Cl_y + \alpha Br_y$ exhibited by the MRI model is due to the high concentrations of ClO in this model, attributed in part to the neglect of the ClO + OH → HCl + O_2 channel. Including this reaction has been shown to produce better agreement with various observations [*Chandra et al.*, 1995].

[33] The reason for the high sensitivity of O_3 to $Cl_y + \alpha Br_y$ within the CNRM-ACM model is not known. For most altitudes, ClO within CNRM-ACM is simulated well by the PSS model. CNRM-ACM does simulate much higher values of ClO just above the tropopause than are accounted for by the PSS simulation; within CNRM-ACM, it appears that chlorine activation is occurring for warmer conditions than suggested by the PSS comparison. The high ClO just above the tropopause cannot explain the large sensitivity of O_3 within this model to $Cl_y + \alpha Br_y$ shown in Figures 2d, 3d, and 4a. We have examined profiles of BrO within the CNRM-ACM and the PSS model (data not shown); we do not believe, based on this comparison, that the high sensitivity of O_3 to halogens exhibited by CNRM-ACM is due to the calculation of BrO within this CCM. It is important to note that the PSS comparisons were done for the REF-B1 simulation (1960–2000, observed aerosols), whereas the bulk of this analysis is based on the REF-B2 simulation (1960–2100, background aerosols). Finally, our comparisons cannot reveal possible errors in the coding of a rate constant that would affect the rate of ozone loss by ClO or BrO but not affect the abundance of ClO or BrO (i.e., the reaction of ClO + O). The reason for the high sensitivity of O_3 to $Cl_y + \alpha Br_y$ within the CNRM-ACM model remains unexplained.

[34] We performed an analysis of the statistical uncertainty from the MLR for the regression variable sensitivities as described by *Oman et al.* [2010] and found similar results (data not shown). In addition, we have added the impact of autocorrelation of the residual on the uncertainty of the individual sensitivities [*Tiao et al.*, 1990, their Appendix A].

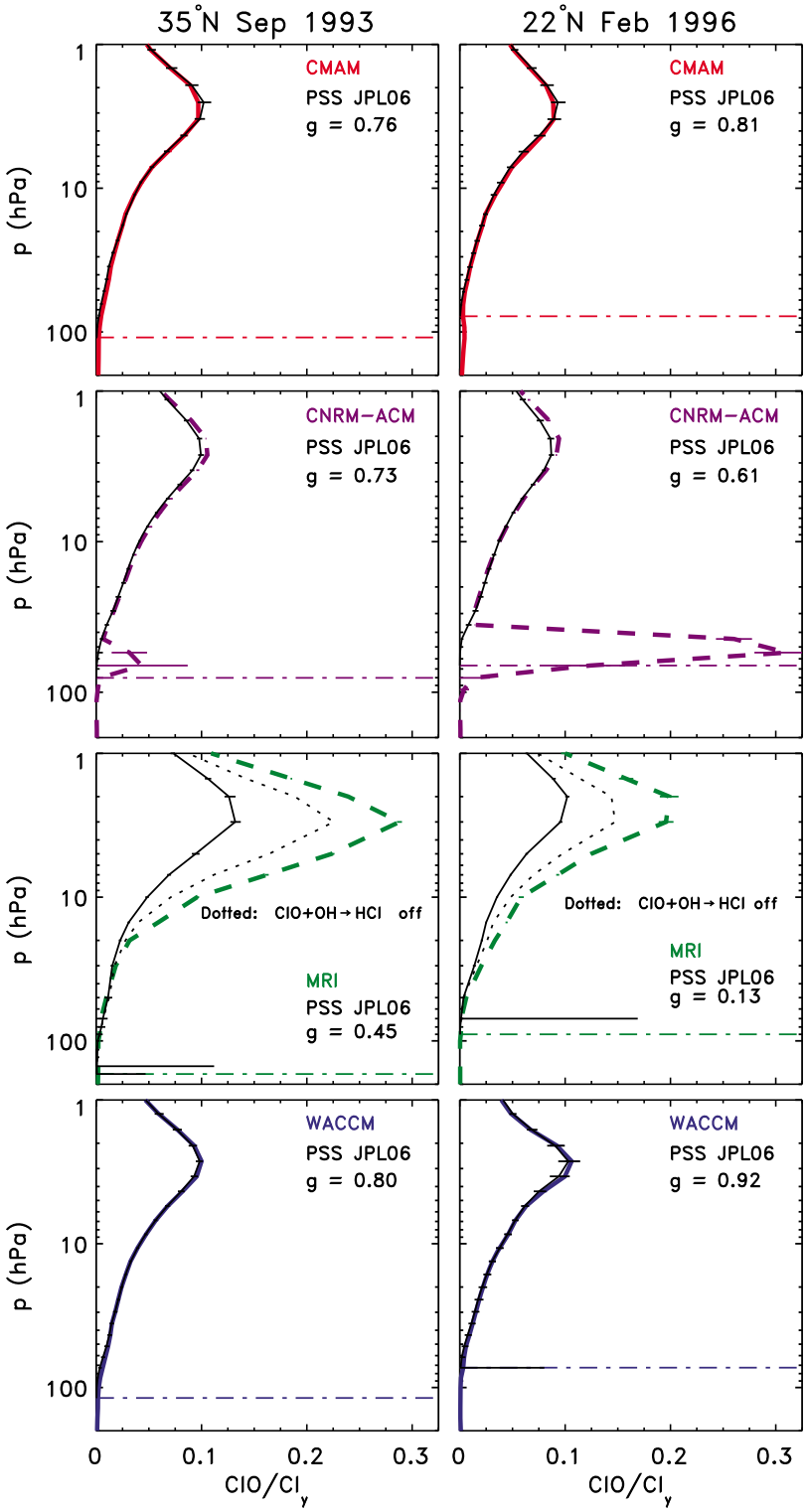

Figure 5. Comparison of zonal, monthly mean profiles of radicals from CCM models (colored lines) versus 24 hour average radical profiles found using a PSS box model constrained by profiles of temperature, O_3, H_2O, CH_4, CO, NO_y, Cl_y, Br_y, and sulfate SAD from the various CCMs for the two indicated times and locations. The PSS model was run at CCM model levels from the tropopause (dashed dotted colored lines) to 1 hPa. All simulations used JPL 2006 kinetics. The colored error bars represent the standard deviation about the zonal monthly mean for various days used to compute the mean. The black error bars represent the sensitivity of PSS output to variability in the CCM profiles of radical precursors. The metrics (values of g) were found as described in chapter 6 of *SPARC CCMVal* [2010]. For the MRI model, PSS simulations are shown with and without loss of ClO by the reaction $ClO + OH \rightarrow HCl + O_2$.

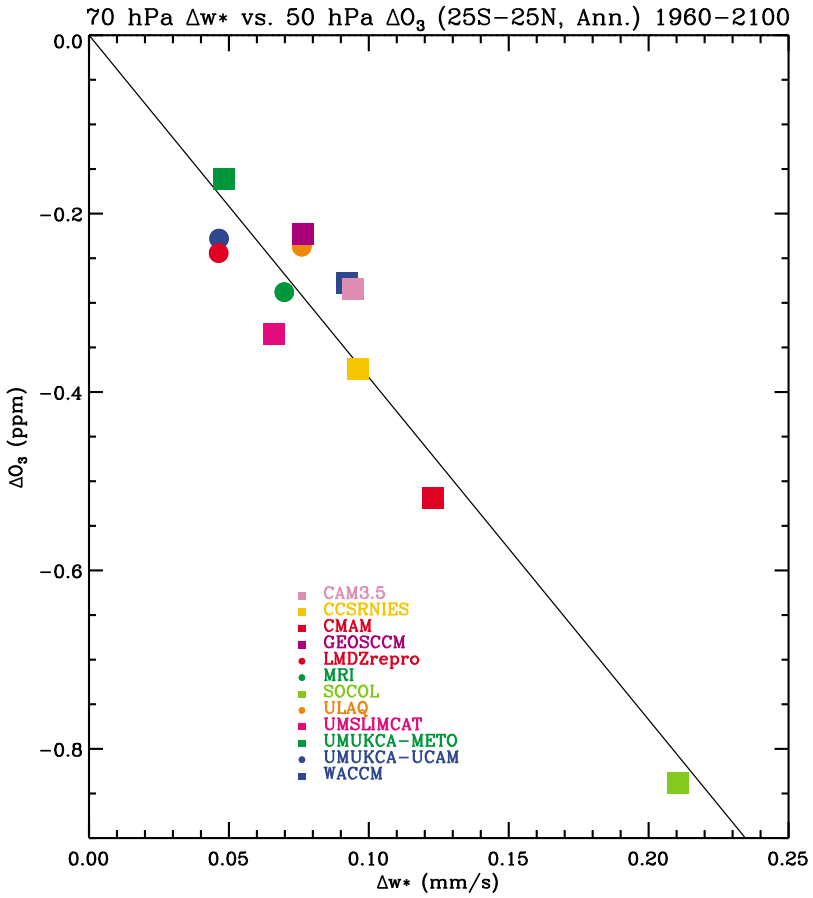

Figure 6. Scatterplot showing the change (from 1960 to 2100) in 70 hPa w* and 50 hPa ozone. The values are annual averages over 25°S–25°N for 12 of the CCMVal models, with the black line showing the linear fit. UMUKCA-METO change is shown from 1960 to 2083.

In the middle to upper stratosphere, there is relatively more uncertainty in the sensitivity of ozone to NO_y compared to much smaller uncertainty associated with sensitivity of ozone to $Cl_y + \alpha Br_y$ and temperature (also shown in Table 2). The larger uncertainty in the sensitivity to NO_y could be due to NO_y being less correlated with ozone variations than for the other explanatory variables. In general, in the lower stratosphere, from 100 to 60 hPa, the sensitivities are not statistically significantly different from zero. The most statistically significant sensitivities typically are found from 10 to 1 hPa for all explanatory variables except HO_x. For HO_x, the sensitivity is low (statistically indistinguishable from zero) at all altitudes except near the stratopause for most models.

[35] The evolution of upper stratospheric ozone and of the different contributing ozone loss mechanisms at midlatitudes is very similar to that in the tropics (data not shown). There are reasonably balanced, nearly equal contributions of $Cl_y + \alpha Br_y$ and temperature changes in the midlatitude upper stratosphere as was found for the tropics. Again, MRI and CNRM-ACM stand out with much larger contributions from $Cl_y + \alpha Br_y$ to ozone changes.

3.4. Lower Stratosphere

[36] As shown in Figure 1, the evolution of ozone in the tropical lower stratosphere ($p > 20$ hPa) differs from that in the upper portion. This can also be seen in the profiles shown in Figure 3b.

[37] Although an MLR analysis has been applied to the lower stratosphere, interpretation of these results is complicated by the large role of transport changes and the tight coupling of upwelling and temperature. In the tropical lower stratosphere, the loss that the MLR attributes to a temperature change is actually largely a response to increased upwelling, which acts to decrease ozone. This is consistent with *Avallone and Prather* [1996], who showed that changes in upwelling are dominant in controlling tropical lower stratospheric ozone. Temperatures can be reduced by both increases in upwelling and decreased ozone. Previous studies have shown that an increase in the tropical upwelling is the principal cause of a decrease in tropical ozone [*Shepherd*, 2008; *Li et al.*, 2009] with an additional possibly smaller contribution from "reverse self-healing" [*Rosenfield et al.*, 2002]. Reverse self-healing occurs as upper stratospheric ozone rises above historical levels causing less ultraviolet radiation to penetrate into the lower stratosphere resulting in the decreased production of ozone.

[38] Since we do not have a transport proxy in the MLR analysis and there is significant temperature-upwelling coupling, we do not perform a detailed analysis of the MLR results in the lower stratosphere. Instead, we look at the correlation between upwelling and ozone changes in the

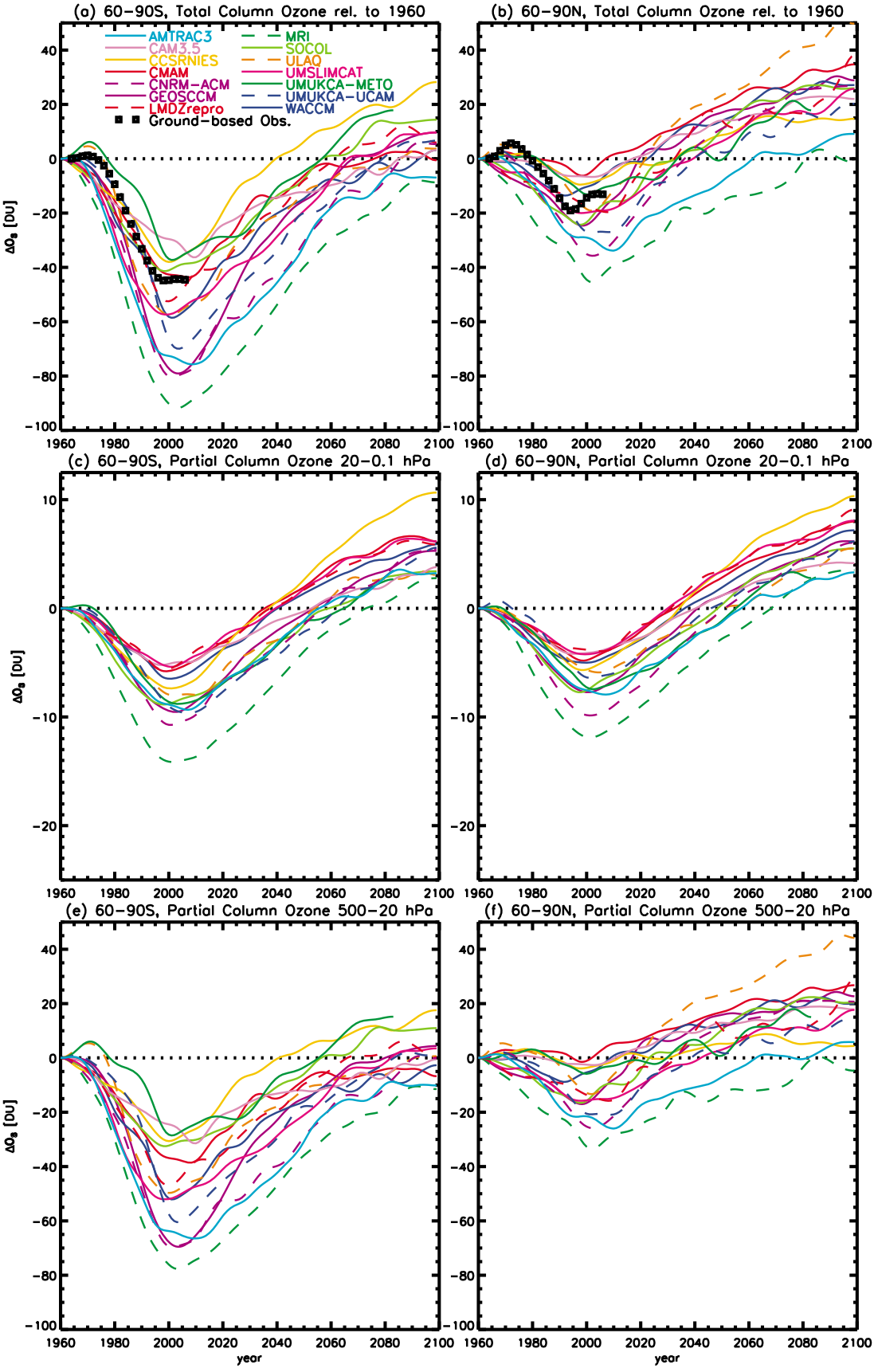
(a) 60–90S, Total Column Ozone rel. to 1960
(b) 60–90N, Total Column Ozone rel. to 1960
(c) 60–90S, Partial Column Ozone 20–0.1 hPa
(d) 60–90N, Partial Column Ozone 20–0.1 hPa
(e) 60–90S, Partial Column Ozone 500–20 hPa
(f) 60–90N, Partial Column Ozone 500–20 hPa
AMTRAC3
CAM3.5
CCSRNIES
CMAM
CNRM–ACM
GEOSCCM
LMDZrepro
MRI
SOCOL
ULAQ
UMSLIMCAT
UMUKCA–METO
UMUKCA–UCAM
WACCM
Ground–based Obs.
ΔO3 [DU]
year

Figure 7

CCMVal-2 models. Figure 6 compares the change in tropical ozone (25°S–25°N) at 50 hPa between 1960 and 2100 to the corresponding change in the residual vertical velocity (w*) at 70 hPa, for the 12 models that provided w* fields. We used the w* from the level below that of ozone, since ozone is impacted not only by local changes in upwelling but also by changes below impacting both advection and production. All models show an increase in tropical upwelling and a decrease in ozone over this time period. However, there is a large spread among the models in the change in both quantities. There is a fairly compact relationship between these two quantities, and a linear fit (black line) nearly intersects the origin, indicating that increases in upwelling are the dominant contributor to ozone decreases at this level. Most models indicate increases in upwelling of 0.04–0.10 mm/s and ozone decreases of 0.15–0.35 ppm over this time period. SOCOL appears to stand out from this group with significantly larger increases in upwelling and ozone decreases, which act in concert to produce the very large temperature reductions seen in Figure 3e. The impact of this larger change in upwelling in SOCOL can also clearly be seen in both total column ozone change (Figure 1b) and partial lower stratospheric ozone change (Figure 1h). In general, differences in the change in upwelling explain differences in lower stratosphere tropical ozone in the CCMVal-2 models. Also, this linear relationship exists when using the same level for ozone and w* (both at 50 and 70 hPa). It would be useful in future studies to further explore the impact of changes in transport and ultraviolet radiation on tropical ozone through additional CCM simulations. For example, a series of simulations in which the various controlling parameters are varied individually, and differences in the model output are examined to better isolate cause and effect as well as nonlinearities, would be especially helpful.

[39] In the midlatitude lower stratosphere, transport is also thought to play an important role for ozone changes, which are generally positive over the 21st century; however, the exact role is not quantified in the present analysis (see further discussion below). In the midlatitudes, the MLR analysis was performed, and results are shown in the *SPARC CCMVal* [2010] study. Given the similar response in the upper stratosphere compared to the tropics, the results are not repeated here.

4. Polar Ozone

[40] We now consider changes in polar ozone. *Austin et al.* [2010b] evaluated the CCMVal-2 model simulations of the Antarctic ozone hole in detail and described both the processes that are well simulated and the areas that need additional work. More information on model biases, especially those involving temperature thresholds for polar stratospheric cloud (PSC) formation, are provided by *Austin et al.* [2010b].

[41] We will first focus on annual average changes and then look at a more detailed analysis of spring when the largest ozone depletion is observed. Figure 7 shows the evolution of annual average southern and northern polar ozone for total column ozone (a and b, top), upper partial column (c and d, middle), and lower partial column (e and f, bottom). We show ground-based total column ozone measurements (black squares, updated from *Fioletov et al.* [2002]) with respect to 1964 in Figures 7a and 7b. SBUV MOD observations (data not shown) are only available for the sunlit portion of the year over the polar latitudes, which could lead to differences compared to the annual average model output shown in Figure 7.

[42] Evolution of the upper partial columns is very similar to that of midlatitudes (Figures 1d and 1f). However, the projections of the lower and total columns differ. All models show larger peak ozone loss around 2000 in the southern polar region than in the northern polar region. This is expected and seen in observations, as there is greater PSC formation in the southern polar region and a more stable polar vortex that lasts into spring each year. In general, there are larger increases in ozone amounts by 2100 compared to 1960 in the northern polar region. It is difficult to say quantitatively with the existing simulations how much of the differences seen by 2100 in the total and partial lower stratospheric column ozone are due to variations in polar chemistry, circulation changes, or a combination of the two. Additional simulations with fixed low chlorine concentrations or fixed GHG concentrations could help to quantify the relative impacts.

[43] The largest ozone losses occur in the spring in the lower portion of the stratospheric column, so we focus on this time and region in more detail. Figure 8a shows the Antarctic (60°–90°S) lower stratospheric column ozone for October. Peak ozone loss averages about 100 DU around 2000 with a range from models between 70 and 170 DU. SBUV MOD partial column observations (black triangles) show an ozone loss of about 80–90 DU between 1979 and ~2000. The limitation on the observational reference year could be impacting the comparison as most models show between 20 and 40 DU ozone loss by 1979. We applied a linear regression analysis to the lower stratospheric column ozone amounts to calculate the contribution from $Cl_y + \alpha Br_y$ using $\alpha = 60$.

[44] Figure 8b shows the contribution of $Cl_y + \alpha Br_y$ and the residual (Figure 8c), which is much smaller and, for most models, typically less than ±20 DU. $Cl_y + \alpha Br_y$ dominates the partial column ozone until the end of the 21st century when the residual is, in most cases, of comparable magnitude. As a proxy for changes in the circulation of the stratosphere, we can look at the mean age of stratospheric air. The decrease in mean age of air (i.e., stronger circulation) (Figure 8e) by itself and in combination with upper stratospheric ozone returning to above historical levels acted

Figure 7. Annual average total and partial column ozone amounts over the high latitudes of each hemisphere (60°–90°S and 60°–90°N). The partial column ozone amounts are separated into (c and d) an upper portion from 20 to 0.1 hPa and (e and f) a lower portion from 500 to 20 hPa. All shown are from 1960 to 2100 (except UMUKCA-METO to 2083) and have been smoothed with a 1:2:1 filter iteratively 30 times. Note the scale change in the *y* axis in Figures 7c and 7d. Ground-based (a and b) total column ozone observations (black squares; plotted every other year) are shown from 1964 to 2007 with respect to 1964.

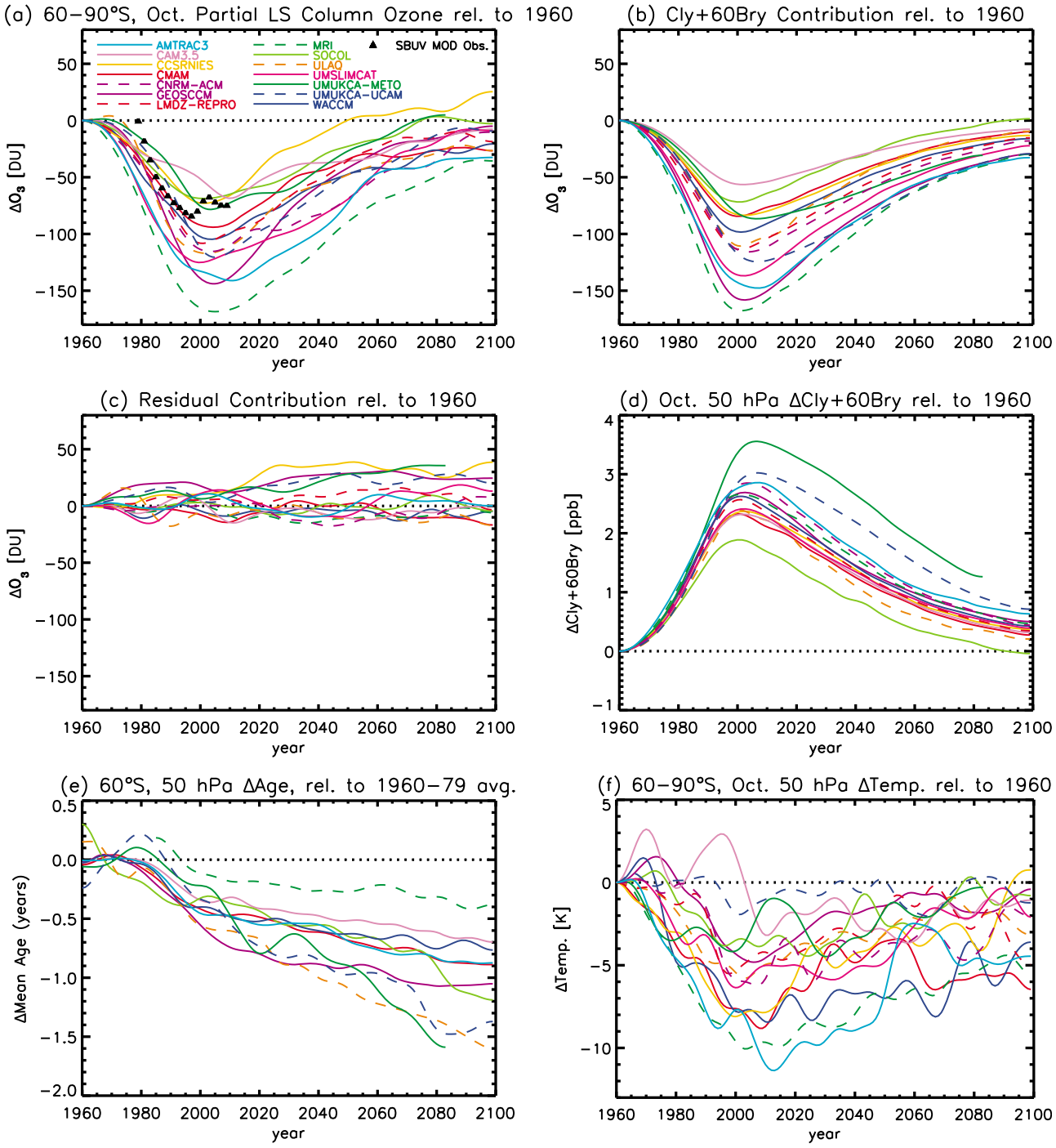

Figure 8. Evolution of ozone for (a) October partial column ozone (500–20 hPa) over 60°–90°S with respect to 1960 levels for the CCMVal models. Model partial column contribution of (b) Cl_y + $60Br_y$ and (c) residual with respect to 1960 levels. Changes in (d) Cl_y + $60Br_y$ at 50 hPa, (e) mean age of air for models that included age of air tracer, and (f) temperature. All shown are from 1960 to 2100 (except UMUKCA-METO to 2083) and have been smoothed with a 1:2:1 filter iteratively 30 times. SBUV MOD partial column ozone observations (black triangles; plotted every other year) are shown over 1979–2009 relative to 1979.

to cause increased ozone change (i.e, positive residual). However, this could be tempered by the cooling of the polar lower stratospheric temperatures (Figure 8f shows 50 hPa temperatures), which occurs in nearly all models.

[45] Figure 9a shows the Arctic (60°–90°N) lower stratospheric column ozone for March. We also note that this area is typically bigger than the size of the polar vortex, so this average also includes mixing effects from the midlatitudes

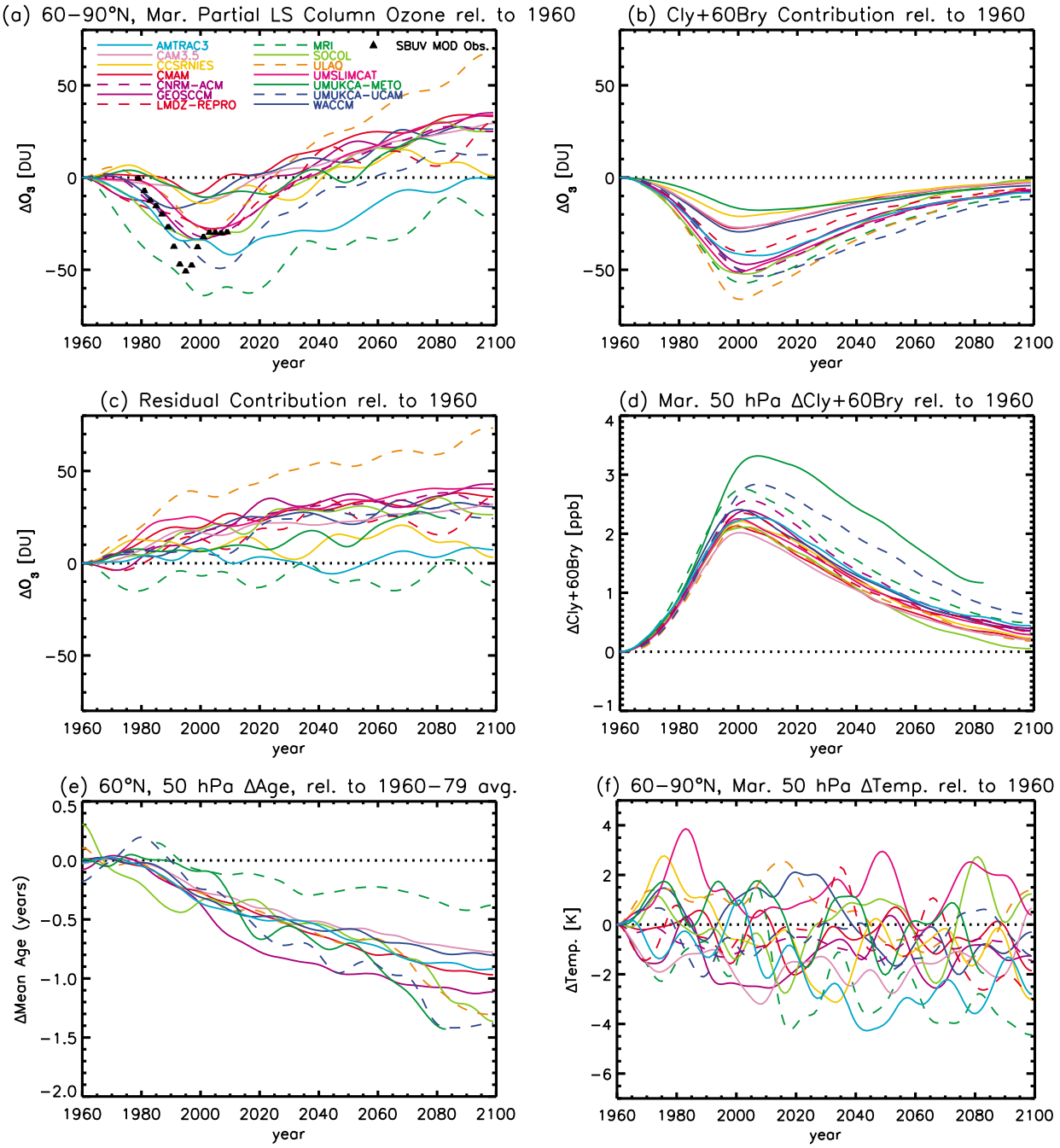

Figure 9. Evolution of ozone for (a) March partial column ozone (500–20 hPa) over 60°–90°N with respect to 1960 levels for the CCMVal models. Model partial column contribution of (b) Cl_y + 60Br_y and (c) residual with respect to 1960 levels. Changes in (d) Cl_y + 60Br_y at 50 hPa, (e) mean age of air for models that included age of air tracer, and (f) temperature. All shown are from 1960 to 2100 (except UMUKCA-METO to 2083) and have been smoothed with a 1:2:1 filter iteratively 30 times. SBUV MOD partial column ozone observations (black triangles; plotted every other year) are shown over 1979–2009 relative to 1979.

(also to a lesser extent in the Southern Hemisphere during October). Peak ozone loss averages at 30 DU around 2000 with a range between 10 and 60 DU. SBUV MOD partial column observations (black triangles) show between 30 and 50 DU loss. Again, we linearly regressed the Cl_y + αBr_y against the partial lower stratospheric column ozone. Figure 9b shows the contribution of Cl_y + αBr_y and the residual (Figure 9c), which in this case is generally larger than in the Antarctic with a consistent 20–40 DU residual by 2100 for most models. This seems to indicate that in the

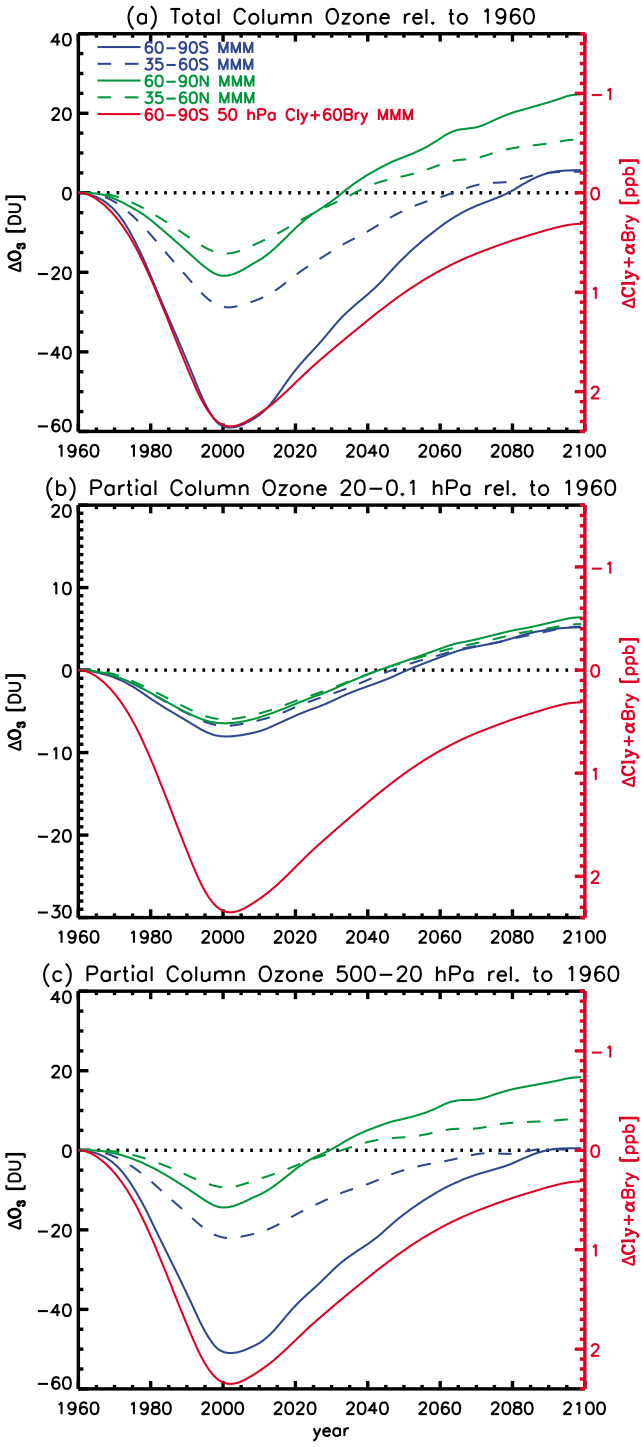

Figure 10. MMM of (a) total and (b and c) partial column ozone amounts for middle (35°–60°S and 35°–60°N; dashed curves) and high (60°–90°S and 60°–90°N; solid curves) latitudes and Cly + αBry for high latitudes (60°–90°S) for reference.

NH polar regions, circulation changes cause a larger increase in ozone than seen in the SH by 2100.

5. Ozone Recovery

[46] The above differences in ozone return dates between regions are summarized in Figure 10, which shows the evolution of the multimodel mean (MMM) total and partial column ozone, with respect to 1960 for high latitudes (solid curves) and midlatitudes (dashed curves). Total column ozone for the MMM (Figure 10a) shows a return to 1960 values by the 2030s in the NH in both middle and high latitudes. In the SH, the total column ozone MMM exhibits a return to 1960 values by the 2060s in the midlatitudes and by 2080 at high latitudes. Nearly all the differences in total column ozone evolution are from the lower portion of the column (500–20 hPa) (Figure 10c) with very similar changes in both hemispheres occurring in the upper portion (Figure 10b). For a more in-depth discussion of return dates, especially with respect to 1980 values, see the study by *Austin et al.* [2010a].

[47] We see a significant difference in the dates ozone and halogens return to historical levels (i.e., 1960 levels). The MMM Cly + αBry does not return to 1960 values by 2100. This is later than the return of ozone (for extratropical regions). The cause of the earlier return of ozone in midlatitudes [*Austin et al.*, 2010a, Figure 16] in both hemispheres is likely from an increased circulation [*Austin and Wilson*, 2006; *Waugh et al.* 2009; *Li et al.*, 2009] along with increased upper stratospheric ozone from stratospheric cooling. The impact of circulation changes on the midlatitude ozone return date is discussed in more detail by *Austin et al.* [2010a].

[48] There is a noticeable difference in the dates when Northern and Southern Hemisphere ozone returns to 1960 values (with no such difference in Cly + αBry; data not shown). This interhemispheric difference is likely caused by asymmetries in transport between the two hemispheres. Some of the delay in the SH return is likely from asymmetries in polar ozone loss since there is significant polar ozone loss occurring in the SH in the early 21st century when NH ozone is returning to 1980 levels (not shown with reference to 1980 levels), causing less ozone to be transported into SH midlatitudes when the vortex breaks down [*Atkinson et al.*, 1989]. The impact of polar ozone losses being transported into the midlatitudes likely plays the dominant role in the later return to historical values seen in models in the SH midlatitudes during first half of the 21st century with any asymmetries in the strengthening of the stratospheric circulation likely having a larger impact toward the later half of the 21st century.

6. Conclusions

[49] Simulations of the past and future were performed using 14 chemistry-climate models for the CCMVal-2 activity. *Austin et al.* [2010a] examined the evolution of total column ozone and compared the recovery of column ozone and Cl_y in these models. Here we have contrasted the evolution in the upper and lower stratosphere and used MLR in the tropics to attribute ozone changes to the predictors with a particular focus on the 21st century.

[50] The simulations presented here and by *Austin et al.* [2010a] show that there is some general agreement in the ozone evolution among the models, with all showing column ozone decreasing from 1960 to around 2000 and then increasing over the first half of the 21st century. Models also show that the column ozone evolution varies with latitude, especially in the latter half of the 21st century. There are

clearly some quantitative differences in ozone evolution across the CCMVal-2 simulations, e.g., a large spread in simulated return of ozone to historical values [*Austin et al.*, 2010a].

[51] Separation into partial columns above and below 20 hPa reveals that the latitudinal differences in the evolution of the column ozone are almost completely attributed to differences in the lower stratosphere (the region of the atmosphere below 20 hPa). In all models, there are only weak latitudinal variations in the evolution of upper stratospheric ozone, and at all latitudes, upper stratospheric ozone increases throughout the 21st century and returns to 1960 levels well before the end of the century. There is, however, a large spread in dates of return to historical values, with, for example, dates of return to 1960 levels at 5 hPa varying from 2020s to 2060s. Over the 21st century, a multiple linear regression analysis indicates that the upper stratospheric ozone increase comes from almost equal contributions of decreases in halogens ($Cl_y + \alpha Br_y$) and cooling from increased greenhouse gas concentrations (for the A1B greenhouse gas scenario considered in these simulations), with only small contributions from NO_y and HO_x. This result depends on the greenhouse gas scenario. Larger changes in N_2O and CH_4 (source gases of NO_y and HO_x, respectively) than considered here could impact the relative contributions from NO_y and HO_x, as shown by *Oman et al.* [2010]. It is also important to keep in mind the limitations of the MLR analysis discussed in section 2.2 when considering these results.

[52] In the tropical lower stratosphere, there is a steady decrease in ozone through the 21st century in all models, whereas ozone in middle and high latitudes increases during the 21st century. As a consequence of increased tropical upwelling induced by rising levels of GHGs, modeled tropical column ozone does not return to 1960 levels even by the end of the century, whereas extratropical ozone returns or is close to 1960 levels well before the end of the century. In the model simulations, while the largest decreases in partial lower stratospheric ozone columns occur during the second half of the 21st century, some smaller decreases are already evident over the recent past. However, ground-based and SBUV satellite observations of total and partial tropical lower stratospheric ozone columns do not show this decrease. *Randel and Wu* [2007] reported negative trends in tropical lower stratospheric ozone using SAGE I and SAGE II data. More work should be done to understand the actual time history of tropical, lower stratospheric ozone to enable a more meaningful comparison to modeled trends. Models with larger future ozone decreases have larger increases in tropical upwelling. Changes in transport also play an important role in the evolution of midlatitude lower stratospheric ozone and contribute to the earlier return of ozone to specific historical values than is found for $Cl_y + \alpha Br_y$.

[53] There are quantitative differences between the hemispheres in the simulated ozone evolution. In particular, ozone returns to historical values earlier in the Northern Hemisphere. This difference in hemispheric return dates varies between 20 and 50 years depending on the latitude of interest for the 1960 reference year chosen, and it is almost completely related to differences in the lower stratosphere. Additional simulations would need to be completed to quantitatively attribute causes for hemispheric differences. However, based on existing simulations, it appears that the larger ozone loss from polar chemistry in the SH and the transport of this ozone-depleted air into the midlatitudes as the vortex breaks down is one cause, especially during the first half of the 21st century. Changes in the stratospheric circulation could also play a role in these differences.

[54] At high latitudes, especially in the SH (Figure 8), $Cl_y + \alpha Br_y$ dominates long-term trends in the lower portion of the column ozone (and total column ozone) with a small (generally positive) residual. This residual is likely caused by circulation changes and upper stratospheric return to above-historical levels.

[55] These results reinforce the conclusions of *Eyring et al.* [2007] using simulations from the CCMVal-1 activity: decreasing levels of halogens, continued stratospheric cooling, and changes in circulation are the major factors driving 21st century ozone trends. It is important to keep in mind that all of these simulations are based on a single GHG and halogen scenario, with only one model including an interactive ocean. In addition, the use of mixing ratio-based halogen boundary conditions rather than emission-based constrains the model's response [*Douglass et al.*, 2008]. Future work should be done to explore these issues and their impact on ozone evolution in more detail.

[56] **Acknowledgments.** This research was supported by the NASA MAP, ACMAP, and Aura programs and the NSF Large-scale Climate Dynamics program. We thank Susan Strahan for very helpful comments on this manuscript, and we thank three anonymous reviewers for thoughtful, constructive reviews of the submitted paper. We acknowledge the Chemistry-Climate Model Validation (CCMVal) Activity of the WCRP SPARC project for organizing and coordinating the model data analysis activity and the British Atmospheric Data Centre for collecting and archiving the CCMVal model outputs. CCSRNIES research was supported by the Global Environmental Research Fund of the Ministry of the Environment of Japan (A-071 and A-0903), and simulations were completed with the supercomputer at CGER, NIES. The MRI simulation was made with the supercomputer at the National Institute for Environmental Studies, Japan. The contribution from the Met Office Hadley Centre was supported by the Joint DECC and Defra Integrated Climate Programme-DECC/Defra (GA01101). The contribution from the LATMOS-IPSL was supported by the European Commission through the funding of the RECONCILE and GEOMON projects. The National Center for Atmospheric Research is operated by the University Corporation for Atmospheric Research under sponsorship of the National Science Foundation. Any opinions, findings, and conclusions or recommendations expressed in the publication are those of the authors and do not necessarily reflect the views of the National Science Foundation.

References

Akiyoshi, H., L. B. Zhou, Y. Yamashita, K. Sakamoto, M. Yoshiki, T. Nagashima, M. Takahashi, J. Kurokawa, M. Takigawa, and T. Imamura (2009), A CCM simulation of the breakup of the Antarctic polar vortex in the years 1980–2004 under the CCMVal scenarios, *J. Geophys. Res.*, *114*, D03103, doi:10.1029/2007JD009261.

Akiyoshi, H., Y. Yamashita, K. Sakamoto, L. B. Zhou, and T. Imamura (2010), Recovery of stratospheric ozone in calculations by the Center for Climate System Research/National Institute for Environmental Studies chemistry-climate model under the CCMVal-REF2 scenario and a no-climate-change run, *J. Geophys. Res.*, *115*, D19301, doi:10.1029/2009JD012683.

Atkinson, R. J., W. A. Matthews, P. A. Newman, and R. A. Plumb (1989), Evidence of the mid-latitude impact of Antarctic ozone depletion, *Nature*, *340*, 290–294, doi:10.1038/340290a0.

Austin, J., and R. J. Wilson (2006), Ensemble simulations of the decline and recovery of stratospheric ozone, *J. Geophys. Res.*, *111*, D16314, doi:10.1029/2005JD006907.

Austin, J., and R. J. Wilson (2010), Sensitivity of polar ozone to sea surface temperatures and halogen amounts, *J. Geophys. Res.*, *115*, D18303, doi:10.1029/2009JD013292.

Austin, J., et al. (2010a), Decline and recovery of total column ozone using a multimodel time series analysis, *J. Geophys. Res.*, *115*, D00M10, doi:10.1029/2010JD013857.

Austin, J., et al. (2010b), Chemistry-climate model simulations of spring Antarctic ozone, *J. Geophys. Res.*, *115*, D00M11, doi:10.1029/2009JD013577.

Avallone, L. M., and M. J. Prather (1996), Photochemical evolution of ozone in the lower tropical stratosphere, *J. Geophys. Res.*, *101*(D1), 1457–1461, doi:10.1029/95JD03010.

Brasseur, G., and M. H. Hitchman (1988), Stratospheric response to trace gas perturbations: Changes in ozone and temperature distributions, *Science*, *240*, 634–637, doi:10.1126/science.240.4852.634.

Butchart, N., and A. A. Scaife (2001), Removal of chlorofluorocarbons by increased mass exchange between the stratosphere and troposphere in a changing climate, *Nature*, *410*, doi:10.1038/35071047.

Butchart, N., et al. (2006), Simulations of anthropogenic change in the strength of the Brewer-Dobson circulation, *Clim. Dyn.*, *27*, 727–741, doi:10.1007/s00382-006-0162-4.

Canty, T., H. M. Pickett, R. J. Salawitch, K. W. Jucks, W. A. Traub, and J. W. Waters (2006), Stratospheric and mesospheric HOx: Results from Aura MLS and FIRS-2, *Geophys. Res. Lett.*, *33*, L12802, doi:10.1029/2006GL025964.

Chandra, S., C. H. Jackman, and E. L. Fleming (1995), Recent trends in ozone in the upper stratosphere: Implications for chlorine chemistry, *Geophys. Res. Lett.*, *22*(7), 843–846, doi:10.1029/94GL03395.

Chipperfield, M. P., and W. Feng (2003), Comment on: "Stratospheric ozone depletion at northern mid-latitudes in the 21st century: The importance of future concentrations of greenhouse gases nitrous oxide and methane," *Geophys. Res. Lett.*, *30*(7), 1389, doi:10.1029/2002GL016353.

Daniel, J. S., S. Solomon, R. W. Portmann, and R. R. Garcia (1999), Stratospheric ozone destruction: The importance of bromine relative to chlorine, *J. Geophys. Res.*, *104*(D19), 23,871–23,880, doi:10.1029/1999JD900381.

Davies, T., M. J. P. Cullen, A. J. Malcolm, M. H. Mawson, A. Staniforth, A. A. White, and N. Wood (2005), A new dynamical core for the Met Office's global and regional modelling of the atmosphere, *Q. J. R. Meteorol. Soc.*, *131*, 1759–1782, doi:10.1256/qj.04.101.

de Grandpré, J., S. R. Beagley, V. I. Fomichev, E. Griffioen, J. C. McConnell, A. S. Medvedev, and T. G. Shepherd (2000), Ozone climatology using interactive chemistry: Results from the Canadian Middle Atmosphere Model, *J. Geophys. Res.*, *105*(D21), 26,475–26,491, doi:10.1029/2000JD900427.

Déqué, M. (2007), Frequency of precipitation and temperature extremes over France in an anthropogenic scenario: Model results and statistical correction according to observed values, *Global Planet. Change*, *57*, 16–26, doi:10.1016/j.gloplacha.2006.11.030.

Douglass, A. R., R. S. Stolarski, M. R. Schoeberl, C. H. Jackman, M. L. Gupta, P. A. Newman, J. E. Nielsen, and E. L. Fleming (2008), Relationship of loss, mean age of air and the distribution of CFCs to stratospheric circulation and implications for atmospheric lifetimes, *J. Geophys. Res.*, *113*, D14309, doi:10.1029/2007JD009575.

Eyring, V., et al. (2005), A strategy for process-oriented validation of coupled chemistry-climate models, *Bull. Am. Meteorol. Soc.*, *86*, 1117–1133, doi:10.1175/BAMS-86-8-1117.

Eyring, V., et al. (2006), Assessment of temperature, trace species, and ozone in chemistry-climate model simulations of the recent past. *J. Geophys. Res.*, *111*, D22308, doi:10.1029/2006JD007327.

Eyring, V., et al. (2007), Multimodel projections of stratospheric ozone in the 21st century, *J. Geophys. Res.*, *112*, D16303, doi:10.1029/2006JD008332.

Eyring, V., P. M. de F. Forster, P. A. Newman, M. Rex, R. J. Salawitch, and B. D. Santer (2008), Report on the Third SPARC CCMVal Workshop, SPARC Newsl., no. 30, pp. 17–19.

Fioletov, V. E., et al. (2002), Global ozone and zonal total ozone variations estimated from ground-based and satellite measurements: 1964–2000, *J. Geophys. Res.*, *107*(D22), 4647, doi:10.1029/2001JD001350.

Garcia, R. R., and W. J. Randel (2008), Acceleration of the Brewer-Dobson circulation due to increases in greenhouse gases, *J. Atmos. Sci.*, *65*, 2731–2739, doi:10.1175/2008JAS2712.1.

Garcia, R. R., D. Marsh, D. E. Kinnison, B. Boville, and F. Sassi (2007), Simulations of secular trends in the middle atmosphere, 1950–2003, *J. Geophys. Res.*, *112*, D09301, doi:10.1029/2006JD007485.

Haigh, J. D., and J. A. Pyle (1979), A two-dimensional calculation including atmospheric carbon dioxide and stratospheric ozone, *Nature*, *279*, 222–224, doi:10.1038/279222a0.

Hegglin, M. I., and T. G. Shepherd (2009), Large climate-induced changes in ultraviolet index and stratosphere-to-troposphere ozone flux, *Nat. Geosci.*, *2*, 687–691, doi:10.1038/ngeo604.

Intergovernmental Panel on Climate Change (IPCC) (2000), *Special Report on Emissions Scenarios: A Special Report of Working Group III of the Intergovernmental Panel on Climate Change*, 599 pp., Cambridge Univ. Press, Cambridge, U. K.

Jackman, C. H., R. S. Stolarski, and J. A. Kaye (1986), Two-dimensional monthly average ozone balance from limb infrared monitor of the stratosphere and stratospheric and mesospheric sounder data, *J. Geophys. Res.*, *91*(D1), 1103–1116, doi:10.1029/JD091iD01p01103.

Jourdain, L., S. Bekki, F. Lott, and F. Lefevre (2008), The coupled chemistry-climate model LMDz-REPROBUS: Description and evaluation of a transient simulation of the period 1980–1999, *Ann. Geophys.*, *26*(6), 1391–1413, doi:10.5194/angeo-26-1391-2008.

Lamarque, J.-F., D. E. Kinnison, P. G. Hess, and F. M. Vitt (2008), Simulated lower stratospheric trends between 1970 and 2005: Identifying the role of climate and composition changes, *J. Geophys. Res.*, *113*, D12301, doi:10.1029/2007JD009277.

Li, F., R. S. Stolarski, and P. A. Newman (2009), Stratospheric ozone in the post-CFC era, *Atmos. Chem. Phys.*, *9*, 2207–2213, doi:10.5194/acp-9-2207-2009.

Morgenstern, O., P. Braesicke, F. M. O'Connor, A. C. Bushell, C. E. Johnson, S. M. Osprey, and J. A. Pyle (2009), Evaluation of the new UKCA climate-composition model. Part 1: The stratosphere, *Geosci. Model Dev.*, *2*, 43–57, doi:10.5194/gmd-2-43-2009.

Morgenstern, O., et al. (2010), Review of the formulation of present-generation stratospheric chemistry-climate models and associated external forcings, *J. Geophys. Res.*, *115*, D00M02, doi:10.1029/2009JD013728.

Oman, L., D. W. Waugh, S. R. Kawa, R. S. Stolarski, A. R. Douglass, and P. A. Newman (2010), Mechanisms and feedbacks causing changes in upper stratospheric ozone in the 21st century, *J. Geophys. Res.*, *115*, D05303, doi:10.1029/2009JD012397.

Pawson, S., R. S. Stolarski, A. R. Douglass, P. A. Newman, J. E. Nielsen, S. M. Frith, and M. L. Gupta (2008), Goddard Earth Observing System chemistry-climate model simulations of stratospheric ozone-temperature coupling between 1950 and 2005, *J. Geophys. Res.*, *113*, D12103, doi:10.1029/2007JD009511.

Pitari, G., E. Mancini, V. Rizi, and D. T. Shindell (2002), Impact of future climate and emission changes on stratospheric aerosols and ozone, *J. Atmos. Sci.*, *59*(3), 414–440, doi:10.1175/1520-0469(2002)059<0414:IOFCAE>2.0.CO;2.

Portmann, R. W., and S. Solomon (2007), Indirect radiative forcing of the ozone layer during the 21st century, *Geophys. Res. Lett.*, *34*, L02813, doi:10.1029/2006GL028252.

Randel, W. J., and F. Wu (2007), A stratospheric ozone profile data set for 1979–2005: Variability, trends, and comparisons with column ozone data, *J. Geophys. Res.*, *112*, D06313, doi:10.1029/2006JD007339.

Randeniya, L. K., P. F. Vohralik, and I. C. Plumb (2002), Stratospheric ozone depletion at northern mid latitudes in the 21st century: The importance of future concentrations of greenhouse gases nitrous oxide and methane, *Geophys. Res. Lett.*, *29*(4), 1051, doi:10.1029/2001GL014295.

Ravishankara, A. R., J. S. Daniel, and R. W. Portmann (2009), Nitrous oxide (N_2O): The dominant ozone-depleting substance emitted in the 21st century, *Science*, *326*, 123–125, doi:10.1126/science.1176985.

Rayner, N. A., D. E. Parker, E. B. Horton, C. K. Folland, L. V. Alexander, D. P. Rowell, E. C. Kent, and A. Kaplan (2003), Global analyses of sea surface temperature, sea ice, and night marine air temperature since the late nineteenth century, *J. Geophys. Res.*, *108*(D14), 4407, doi:10.1029/2002JD002670.

Rind, D., D. Shindell, P. Lonergan, and N. K. Balachandran (1998), Climate change in the middle atmosphere. Part III: The doubled CO2 climate revisited, *J. Clim.*, *11*, 876–894, doi:10.1175/1520-0442(1998)011<0876:CCATMA>2.0.CO;2.

Rosenfield, J. E., and A. R. Douglass (1998), Doubled CO_2 effects on NO_y in a coupled 2-D model, *Geophys. Res. Lett.*, *25*(23), 4381–4384, doi:10.1029/1998GL900147.

Rosenfield, J. E., A. R. Douglass, and D. B. Considine (2002), The impact of increasing carbon dioxide on ozone recovery, *J. Geophys. Res.*, *107*(D6), 4049, doi:10.1029/2001JD000824.

Santee, M. L., I. A. MacKenzie, G. L. Manney, M. P. Chipperfield, P. F. Bernath, K. A. Walker, C. D. Boone, L. Froidevaux, N. J. Livesey, and J. W. Waters (2008a), A study of stratospheric chlorine partitioning based on new satellite measurements and modeling, *J. Geophys. Res.*, *113*, D12307, doi:10.1029/2007JD009057.

Santee, M. L., et al. (2008b), Validation of the Aura Microwave Limb Sounder ClO measurements, *J. Geophys. Res.*, *113*, D15S22, doi:10.1029/2007JD008762.

Schraner, M., et al. (2008), Technical Note: Chemistry-climate model SOCOL: Version 2.0 with improved transport and chemistry/microphysics schemes, *Atmos. Chem. Phys.*, *8*, 5957–5974, doi:10.5194/acp-8-5957-2008.

Scinocca, J. F., N. A. McFarlane, M. Lazare, J. Li, and D. Plummer (2008), Technical note: The CCCma third generation AGCM and its extension

into the middle atmosphere, *Atmos. Chem. Phys.*, *8*, 7055–7074, doi:10.5194/acp-8-7055-2008.

Scinocca, J. F., D. B. Stephenson, T. C. Bailey, and J. Austin (2010), Estimates of past and future ozone trends from multimodel simulations using a flexible smoothing spline methodology, *J. Geophys. Res.*, *115*, D00M12, doi:10.1029/2009JD013622.

Shepherd, T. G. (2008), Dynamics, stratospheric ozone, and climate change, *Atmos. Ocean*, *46*, 117–138, doi:10.3137/ao.460106.

Shepherd, T. G., and A. I. Jonsson (2008), On the attribution of stratospheric ozone and temperature changes to changes in ozone-depleting substances and well-mixed greenhouse gases, *Atmos. Chem. Phys.*, *8*, 1435–1444, doi:10.5194/acp-8-1435-2008.

Shibata, K., and M. Deushi (2008a), Long-term variations and trends in the simulation of the middle atmosphere 1980–2004 by the chemistry-climate model of the Meteorological Research Institute, *Ann. Geophys.*, *26*, 1299–1326, doi:10.5194/angeo-26-1299-2008.

Shibata, K., and M. Deushi (2008b), Simulation of the stratospheric circulation and ozone during the recent past (1980–2004) with the MRI chemistry-climate model, *CGER's Supercomp. Monogr. Rep.*, *13*, 154 pp., Cent. for Global Environ. Res., Natl. Inst. for Environ. Studies, Tsukuba, Japan.

Shindell, D. T., D. Rind, and P. Lonergan (1998), Climate change and the middle atmosphere. Part IV: Ozone response to doubled CO_2, *J. Clim.*, *11*, 895–918, doi:10.1175/1520-0442(1998)011<0895:CCATMA>2.0.CO;2.

Shine, K. P., et al. (2003), A comparison of model-simulated trends in stratospheric temperatures, *Q. J. R. Meteorol. Soc.*, *129*, 1565–1588, doi:10.1256/qj.02.186.

SPARC CCMVal (2010), SPARC Report on the Evaluation of Chemistry-Climate Models, edited by V. Erying, T. G. Shepherd, D. W. Waugh (Eds.), *SPARC Rep. 5*, WCRP-132, WMO/TD-No. 1526, http://www.atmosp.physics.utoronto.ca/SPARC.

Stolarski, R. S., and S. M. Frith (2006), Search for evidence of trend slowdown in the long-term TOMS/SBUV total ozone data record: The importance of instrument drift uncertainty, *Atmos. Chem. Phys.*, *6*, 4057–4065, doi:10.5194/acp-6-4057-2006.

Teyssèdre, H., et al. (2007), A new tropospheric and stratospheric chemistry and transport model MOCAGE-Climat for multi-year studies: Evaluation of the present-day climatology and sensitivity to surface processes, *Atmos. Chem. Phys.*, *7*, 5815–5860, doi:10.5194/acp-7-5815-2007.

Tian, W., and M. P. Chipperfield (2005), A new coupled chemistry-climate model for the stratosphere: The importance of coupling for future O_3-climate predictions, *Q. J. R. Meteorol. Soc.*, *131*, 281–303, doi:10.1256/qj.04.05.

Tian, W., M. P. Chipperfield, L. J. Gray, and J. M. Zawodny (2006), Quasi-biennial oscillation and tracer distributions in a coupled chemistry-climate model, *J. Geophys. Res.*, *111*, D20301, doi:10.1029/2005JD006871.

Tiao, G. C., et al. (1990), Effects of autocorrelation and temporal sampling schemes on estimates of trend and spatial correlation, *J. Geophys. Res.*, *95*(D12), 20,507–20,517, doi:10.1029/JD095iD12p20507.

Waugh, D. W., L. Oman, S. R. Kawa, R. S. Stolarski, S. Pawson, A. R. Douglass, P. A. Newman, and J. E. Nielsen (2009), Impact of climate change on stratospheric ozone recovery, *Geophys. Res. Lett.*, *36*, L03805, doi:10.1029/2008GL036223.

World Meteorological Organization (WMO)/United Nations Environment Programme (UNEP) (2003), Scientific Assessment of Ozone Depletion: 2002, World Meteorological Organization, Global Ozone Research and Monitoring Project, *Rep. 47*, World Meteorol. Organ., Geneva, Switzerland.

World Meteorological Organization (WMO)/United Nations Environment Programme (UNEP) (2007), Scientific Assessment of Ozone Depletion: 2006, World Meteorological Organization, Global Ozone Research and Monitoring Project, *Rep. 50*, World Meteorol. Organ., Geneva, Switzerland.

Yang, E.-S., D. M. Cunnold, R. J. Salawitch, M. P. McCormick, J. Russell III, J. M. Zawodny, S. Oltmans, and M. J. Newchurch (2006), Attribution of recovery in lower-stratospheric ozone, *J. Geophys. Res.*, *111*, D17309, doi:10.1029/2005JD006371.

Yang, E.-S., D. M. Cunnold, M. J. Newchurch, R. J. Salawitch, M. P. McCormick, J. M. Russell III, J. M. Zawodny, and S. J. Oltmans (2008), First stage of Antarctic ozone recovery, *J. Geophys. Res.*, *113*, D20308, doi:10.1029/2007JD009675.

Ziemke, J. R., S. Chandra, and P. K. Bhartia (2005), A 25-year data record of atmospheric ozone in the Pacific from Total Ozone Mapping Spectrometer (TOMS) cloud slicing: Implications for ozone trends in the stratosphere and troposphere, *J. Geophys. Res.*, *110*, D15105, doi:10.1029/2004JD005687.

H. Akiyoshi, T. Nakamura, and Y. Yamashita, National Institute for Environmental Studies, Tsukuba 305-8506, Japan.

J. Austin, NOAA Geophysical Fluid Dynamics Laboratory, Princeton, NJ 08540, USA.

S. Bekki, D. Cugnet, and M. Marchand, LATMOS-IPSL, UPMC, Paris F-75252 France.

P. Braesicke and J. Pyle, NCAS-Climate-Chemistry, Centre for Atmospheric Science, Department of Chemistry, University of Cambridge, Cambridge CB2 IEW, UK.

N. Butchart and S. C. Hardiman, Met Office Hadley Centre, Exeter EX1 3PB, UK.

T. Canty and R. J. Salawitch, Department of Chemistry and Biochemistry, University of Maryland, College Park, MD 20742, USA.

M. P. Chipperfield, S. Dhomse, and W. Tian, School of Earth and Environment, University of Leeds, Leeds LS2 9JT, UK.

A. R. Douglass, S. Frith, J. E. Nielsen, L. D. Oman, R. S. Stolarski, and J. R. Ziemke, Atmospheric Chemistry and Dynamics Branch, NASA Goddard Space Flight Center, Code 613.3, Greenbelt, MD 20771, USA. (luke.d.oman@nasa.gov)

V. Eyring, Deutsches Zentrum für Luft- und Raumfahrt, Institut für Physik der Atmosphäre, Oberpfaffenhofen D-82234, Germany.

D. E. Kinnison and J.-F. Lamarque, NCAR, Boulder, CO 80307-3000, USA.

E. Mancini and G. Pitari, Dipartimento di Fisica, University of L'Aquila, L'Aquila I-67010, Italy.

M. Michou, D. Olivié, and H. Teyssèdre, GAME/CNRM, Météo-France, CNRS, Toulouse F-31057, France.

O. Morgenstern, National Institute of Water and Atmospheric Research, Private Bag 50061 Omakau, Lauder 9352, New Zealand.

D. A. Plummer and J. F. Scinocca, Canadian Centre for Climate Modelling and Analysis, Victoria, BC V8W 3V6, Canada.

E. Rozanov, Physical-Meteorological Observatory Davos, World Radiation Center, CH-7260 Davos, Switzerland.

T. G. Shepherd, Department of Physics, University of Toronto, Toronto, ON M5S 1A7, Canada.

K. Shibata, Meteorological Research Institute, Japan Meteorological Agency, Tsukuba, Ibaraki 305-0052, Japan.

D. W. Waugh, Department of Earth and Planetary Sciences, Johns Hopkins University, Baltimore, MD 21218, USA.